

1 **Response of Subantarctic microbes to new versus regenerated Fe** 2 **in a cold-core eddy**

3
4 M. Fourquez^{1,2,3}, R. Strzepek^{1,2}, M.J. Ellwood⁴, C. Hassler⁵, D. Cabanes⁵, S. Eggins⁴, I.
5 Pearce⁶, S. Deppeler^{1,7}, T. Trull^{1,2,8}, P.W. Boyd^{1,2}, M. Bressac^{1,9}

6 ¹ Institute for Marine and Antarctic Studies, University of Tasmania, Hobart, TAS, Australia;

7 ² Antarctic Climate and Ecosystems CRC, University of Tasmania, Hobart, TAS, Australia;

8 ³ Aix Marseille Univ., Université de Toulon, CNRS, IRD, MIO UMR 110, 13288, Marseille,
9 France

10 ⁴ Research School of Earth Sciences, Australian National University, Canberra, Australia;

11 ⁵ Marine and Lake Biogeochemistry, Department F.-A. Forel, University of Geneva, Geneva,
12 Switzerland

13 ⁶ Australian Antarctic Division, AAD, Kingston, TAS, Australia;

14 ⁷ National Institute of Water and Atmospheric Research, Wellington, New Zealand;

15 ⁸ Climate Science Centre, Oceans and Atmosphere, Commonwealth Scientific and Industrial
16 Research Organisation, Hobart, TAS, Australia.

17 ⁹Sorbonne Université, CNRS, Laboratoire d'Océanographie de Villefranche, LOV,
18 Villefranche-sur-Mer, 06230, France

19

20 **Keywords: Fe regeneration, particles, Southern ocean eddies, vertical supply,**
21 **Subantarctic**

22 **ABSTRACT**

23 In the Subantarctic sector of the Southern Ocean, vertical entrainment of dissolved iron (DFe)
24 triggers the seasonal productivity cycle. However, diminishing physical supply of new Fe
25 during the spring to summer transition rapidly drives epipelagic microbial communities to rely
26 upon recycled DFe for growth. Hence, subpolar waters evolve seasonally from a high *fe* ratio
27 system (i.e., [uptake of new Fe]/[uptake of new+recycled Fe]) to a low *fe* ratio system. Here,
28 we tested how resident microbes within a cyclonic eddy respond to different Fe/ligand inputs
29 which mimic entrained new DFe (Fe-NEW), diffusively-supplied regenerated DFe (Fe-REG),
30 and a control with no addition of DFe (Fe-NO). After 6 days, 3.5 (Fe-NO, Fe-NEW) to 5-fold
31 (Fe-REG) increases in Chl *a* were observed despite ~2.5-fold range between treatments of
32 initial DFe. Marked differences were also evident in the proportion of *in vitro* DFe derived
33 from recycling to sustain phytoplankton growth (Fe-REG, 30% recycled c.f. 70% Fe-NEW,

34 50% Fe-NO). This trend supports the concept that DFe/ligands released from subsurface
35 particles are more bioavailable than new DFe collected at the same depth. This additional
36 recycling may be mediated by bacteria. Indeed, by day 6 bacterial production (BP) was
37 comparable between Fe-NO and Fe-NEW but ~2 fold higher in Fe-REG. Interestingly, a
38 preferential response of phytoplankton (haptophyte-dominated) relative to bacteria was also
39 found in Fe-REG. In contrast, in Fe-NEW and Fe-NO the proportion of diatoms increased.
40 Hence, different modes of Fe/ligand supply modify BP and Fe bioavailability to phytoplankton
41 that may drive distinctive floristic shifts and biogeochemical signatures.

42

43 **Plain language summary**

44 The Subantarctic Southern Ocean is far away from terrestrial iron inputs. Low dissolved iron
45 (DFe) supply strongly limits the growth of phytoplankton in subpolar surface waters. However,
46 phytoplankton benefit from vertical Fe supply from a subsurface reservoir (termed new Fe)
47 which triggers the beginning of the phytoplankton growth season. However, this entrained new
48 DFe is rapidly consumed and hence relief from Fe stress is only transitory. The relative
49 influence of mid-season diffusive vertical supply and Fe recycling in supporting phytoplankton
50 growth during the transition from new to recycled DFe remains unknown. This study uses a
51 two-step experiment to simulate the seasonal DFe supply pathways for a resident community
52 late in the growth season when cells should be acclimated to low DFe levels. We show that
53 regenerated DFe from subsurface particles enhance secondary production by bacteria and
54 stimulates specific phytoplankton taxa to grow. In particular, we present evidence that small
55 species and non-siliceous cells were better able to take advantage of Fe regenerated from
56 particles than large phytoplankton species. The distinctive stimulation of different microbial
57 pathways driven by different DFe supply mechanisms provides insights into the seasonal
58 signatures of iron biogeochemistry on the subpolar Southern Ocean.

59 1. INTRODUCTION

60 Low concentrations of dissolved iron (DFe) exert a strong influence on the primary
61 productivity across much of the Southern Ocean (SO) (Moore et al., 2001). Nevertheless,
62 widespread phytoplankton blooms occur every year due to the supply of dissolved Fe (DFe)
63 over wide areas of the SO (Thomalla et al., 2011). In early spring, this Fe fertilization is
64 dominated by a one-off pulse of new DFe from the subsurface reservoir through deep winter
65 mixing and entrainment (Nicholson et al., 2019; Tagliabue et al., 2014). This new DFe is
66 rapidly consumed by the upper ocean biota and, as the mixed layer (ML) depth decreases over
67 the season, the diapycnal diffusion of regenerated DFe (from subsurface biological recycling)
68 becomes a major mechanism to extend the duration of summertime production (Boyd et al.,
69 2005, 2017; Tagliabue et al., 2014).

70 Several studies have investigated how the phytoplankton community responds to transient ML
71 deepening (i.e. Arteaga et al., 2020; Rembauville et al., 2017) but confounding effects have
72 hindered our understanding of biological responses to different Fe sources. For example, during
73 late summer - when Fe limitation is at its strongest (Boyd, 2002; Mtshali et al., 2019; Ryan-
74 Keogh et al., 2018) - the response of phytoplankton to transient ML deepening is partly
75 controlled by the degree of Fe limitation relative to light availability (Boyd & Abraham, 2001;
76 Fauchereau et al., 2011). Further, changes in vertical mixing can alter predator-prey
77 interactions (Behrenfeld, 2010) and the effect of ML deepening then becomes more complex
78 than an early season pulse of physically supplied new DFe. Organisms have therefore adapted
79 strategies in response to seasonal changes in Fe availability. At the cellular level, upregulation
80 of Fe transport systems (i.e. Hudson & Morel, 1990; Strzepek et al., 2011; Toulza et al., 2012)
81 and substitution with isofunctional Fe-free proteins (Nunn et al., 2013; Saito et al., 2011;
82 Strzepek & Harrison, 2004) increase Fe uptake rates and decrease the dependence on
83 extracellular Fe, respectively. At the community level, intense grazing- and viral-mediated Fe
84 recycling can account for most of the microbial Fe demand (Boyd et al., 2012; Poorvin et al.,
85 2004; Sarthou et al., 2008; Strzepek et al., 2005).

86 Heterotrophic prokaryotes (here after 'bacteria') play a key role in DFe recycling. Particulate
87 Fe loss during cell lysis can be solubilized in the upper water column by bacteria, which
88 ultimately replenishes the DFe pool (Blain & Tagliabue, 2016 and references herein).
89 Regeneration of DFe by bacteria (termed remineralization) also occurs at depth often on

90 sinking or suspended biogenic particles, which resupplies surface waters through vertical
91 mixing (Boyd et al., 2017; Bressac et al., 2019; Tagliabue et al., 2014). This source of DFe
92 relies heavily upon the efficiency of Fe recycling within the microbial loop (as termed the
93 ‘ferrous wheel’, Kirchman, 1996) that can drive 50 to >90% of Fe-fueled productivity
94 (Strzepek et al., 2005).

95 Within the ferrous wheel, bacteria are also pivotal in setting Fe bioavailability for the entire
96 microbial community. Indeed, most remineralization of organic carbon in the ocean is driven
97 by these microorganisms, a process that returns particulate Fe into dissolved forms (Boyd et
98 al., 2010; Bressac et al., 2019) together with Fe-ligands (Christel S. Hassler et al., 2017; Hunter
99 & Boyd, 2007). Bacteria also represent a large fraction of the biogenic Fe pool and contribute
100 significantly to DFe utilization in the ML (Boyd et al., 2010; Fourquez et al., 2015; Strzepek
101 et al., 2005). Rates of DFe regenerated by bacteria (Boyd et al., 2010, 2012) can effectively
102 meet the high Fe requirements of phytoplankton (Twining & Baines, 2013). However, specific-
103 taxon metabolic strategies amongst phytoplankton are influenced by differences in the mode
104 of DFe supply (Boyd et al., 2017), meaning that bacterially-regenerated sources of DFe may
105 not be bioavailable to all organisms. This raises the following questions: can acclimated surface
106 microbial communities access regenerated Fe? And if some taxa target the supply of new Fe
107 (Boyd et al., 2017), do others focus on recycled forms? These aspects are of particular
108 importance in oceanic features where external Fe sources are not effective, such as persistent
109 strong eddies in the Subantarctic Zone (SAZ; Frenger et al., 2015).

110 In this study, we aimed to address these questions by testing the response of in-eddy resident
111 microbial communities to different Fe supply (and differing ligands) scenarios. Our
112 experimental set-up was based on the seasonal variability of the f_e ratio (i.e., the proportion of
113 Fe uptake from new and regenerated sources, (Boyd et al., 2005). From early spring to late
114 summer, the f_e ratio is projected to decline along with the growing dependency of the biota to
115 access DFe from regenerated sources (Tagliabue et al., 2014). To mimic the supply of
116 subsurface DFe along with the alteration of predator-prey interactions, we simulated changes
117 in top-down control of phytoplankton stocks through dilution. This approach could lead to a
118 decoupling of the predator-prey link in the ferrous wheel. However, it was a necessary step
119 toward investigating the physiological changes, community shifts, and competitive interactions
120 among the different microbial groups (phytoplankton and bacteria) to different DFe sources.
121 Hence, we followed the biological responses of the surface community to the following

122 perturbations: supply of subsurface upwelled new DFe (high fe ratio), diffusive supply from
123 subsurface waters with regenerated DFe (intermediate fe ratio), and ambient surface DFe with
124 high recycling (low fe ratio).

125

126 **2. MATERIAL AND METHODS**

127 **2.1. Environmental context**

128 The study was carried out in April 2016 aboard the RV *Investigator* in the Subantarctic Zone
129 (EDDY cruise, part of the V02-IN2016 voyage from March 11 to April 17, 2016), at the center
130 of a cyclonic cold-core eddy (50.4°S, 147.1°E; 190 km in diameter; Supp. Fig. 1). Eddies are
131 highly variable physical-chemical features in space and time, and can become structurally
132 closed. In late summer 2016, one of these isolated eddies detached from the Subantarctic Front
133 (Patel et al., 2019) and was characterized by an extremely low DFe inventory (Ellwood et al.,
134 2020) and low primary productivity (Moreau et al., 2017). This eddy was sampled in the middle
135 of its lifetime during late summer/earlier fall when biological production is expected to be
136 particularly sensitive to vertical entrainment of new DFe (Ryan-Keogh et al., 2018) and when
137 microbial residents are acclimated to very low Fe concentrations (Tagliabue et al., 2014).
138 Investigations on DFe isotopes inventory confirmed that enhanced bacterially-mediated Fe
139 recycling occurred below 100m depth, and suggested that cells in the euphotic zone also
140 upregulated uptake of Fe and recycling processes to sustain themselves (Ellwood et al., 2020).

141 The study was conducted in two steps, preparation of DFe treatments, followed by
142 manipulation of samples to be incubated. The conceptual basis behind the design of each
143 treatment comes from a proposed seasonal transition from high to low fe ratios outlined in
144 Tagliabue et al. (2014) (see Suppl. Fig. 1). We used this approach to prepare three DFe
145 treatments that represent the hypothetical transition of modes of DFe supply from mainly new
146 DFe early in the season (entrainment), regenerated DFe from the recycling of subsurface
147 materials in summer (diapycnal diffusion), and no supply of DFe (dominance of DFe recycling
148 in surface). In addition to collecting seawater and subsurface particles (see section 2.2) at the
149 center of the eddy (50.4°S, 147.1°E), we collected discrete seawater samples at the edge
150 (49.7°S, 146.4°E) for comparison.

151

152 **2.2.Preparation of three different DFe sources**

153 All manipulations were carried out under strict trace metal-clean conditions in a clean container
154 and in a laminar flow hood. Detailed cleaning procedures to prepare all the labware in trace
155 metal-clean conditions can be found in the Geotraces Cookbook (Cutter et al., 2017).

156 **2.2.1. Source of new DFe**

157 To mimic supply of new DFe (entrainment), deep water samples were collected at 150m depth
158 at the center of the eddy from trace metal clean Niskin bottles deployed on a trace metal rosette.
159 Seawater was directly filtered from the Niskin bottles (transferred into a clean container)
160 through an acid-cleaned 0.2- μ m capsule filter (Suppl. Fig. 2).

161 **2.2.2. Source of regenerated DFe**

162 To mimic supply of regenerated DFe from subsurface materials (diffusion diapycnal) we
163 collected particles at 150m depth at the center of the eddy by *in-situ* filtration (McLane
164 Research Laboratories *in situ* pumps). A total of 345L of seawater passed through acid-leached
165 1.0- μ m polycarbonate (PC) filters (142 mm diameter). The subsurface particles were gently
166 resuspended in a 10L High Density Polyethylene (HDPE) acid-washed bottle containing 7L of
167 <0.2- μ m seawater (acid-cleaned 0.2- μ m capsule filter Supor Acropak 200, Pall) collected at
168 the same depth, resulting in a concentration factor of particles close to 50. For 6 days, the
169 particles with their attached bacteria were incubated in the dark (to avoid photochemical
170 breakdown of ligands), under gentle agitation, and at the *in situ* temperature of 7°C. We assume
171 that (as we concentrated the particulate fraction) mainly attached bacteria were involved in the
172 degradation of the particulates, thereby releasing DFe and ligands in the dissolved phase. The
173 efficiency of bacterial remineralization was assessed over time by measuring total and free-
174 living bacterial production along with changes in nutrient (NH₄, NO₂, NO₃, PO₄, and Si)
175 concentration, including DFe.

176 **2.2.3. Source of surface DFe**

177 For ambient DFe source, surface seawater was collected at 5m depth at the center of the eddy
178 using towed *in situ* sampler and directly filtered through an acid-cleaned 0.2- μ m capsule filter
179 (Supor Acropak 200, Pall).

180

181 **2.2 Incubation of surface microbial community**

182 The surface microbial community was collected from 5m depth at the center of the eddy using
183 a towed fish system and drawn onboard using an air-driven Teflon diaphragm pump.
184 Incubation experiments were set in acid-washed 1L round polycarbonate bottles and consisted
185 of mixing 375 mL of surface seawater with (i) 375 mL of source of new Fe (Fe-NEW
186 treatment), (ii) 375 mL of source of regenerated Fe (Fe-REG treatment), and (iii) 375 mL of
187 source of surface seawater (Fe-NO treatment); leading to a systematic dilution of the surface
188 community by 50% (Suppl. Fig. 2). Twelve independent replicates per treatment were covered
189 with shade cloth ($73 \pm 5\%$ of surface irradiance), placed in an on-deck incubator with
190 continuous seawater supply ($9.9 \pm 1.1^\circ\text{C}$), and harvested after 0, 2, 4 and 6 days.

191 In parallel, we performed additional dark incubations of natural surface communities amended
192 either with 1 nM FeCl_3 (“NO-dark +Fe”) or organic carbon 10 μMC (trace metal-clean glucose,
193 “NO-dark +C”), or a combination of both (“NO-dark +Fe+C”), and followed daily bacterial
194 abundance and heterotrophic production for up to 6 days (Suppl. Fig. 2). Note that in the +Fe+C
195 treatment $16.6 \mu\text{molFe molC}^{-1}$ of nutrients were added to match the bacterial Fe quota
196 observed for Fe-replete bacterial cultures (Fourquez et al., 2014). These incubations were
197 dedicated to determining if single and/or combined additions of Fe and C stimulate bulk and
198 cell-specific bacterial production, and assessing if heterotrophic prokaryotes from the surface
199 ocean were primarily Fe or C-limited. Additional incubations with Fe-NO and Fe-REG waters
200 (NO-dark and REG-dark, respectively) were conducted under the same conditions but with no
201 amendment to compare with products produced during the remineralization of subsurface
202 particles (step 1). Suppl. Figure 2 summarizes the experimental set-up.

203 **2.3. Biological metrics**

204 The biological response of the microbial community (phytoplankton and bacteria) to the three
205 different DFe sources were monitored from these incubation bottles, and analyzed for several
206 parameters as described in sections below. Three biological replicates were used at each time
207 point to get independent data points.

208 **2.3.1. Cell abundances**

209 Enumeration of pico- and nanophytoplankton, cyanobacteria and heterotrophic prokaryotes
210 cells were determined by flow cytometry with similar methods and instrumentation as
211 described in Fourquez et al. (2020). Briefly, 4.5 mL subsamples were fixed with glutaraldehyde
212 (0.5% final concentration) in the dark at 4°C for 20 min, shock-frozen in liquid nitrogen, and

213 stored at -80°C . High (HNA) and low nucleic acid content (LNA) prokaryotes were
214 discriminated depending on their respective signature in the cytogram of green fluorescence
215 versus side scatter. Autotrophic cell populations were separated into regions based on their
216 autofluorescence in red (FL3) versus orange (FL2) bivariate scatter plots. Cyanobacteria were
217 determined from their high FL2 and low FL3 fluorescence. Pico- and nanophytoplankton
218 communities were determined from their relative cell size using side scatter versus FL3
219 bivariate scatter plots.

220 **2.3.2. Pigments composition**

221 Samples (400-600 mL) for pigments were analyzed by HPLC (Wright et al., 2010). Pigments
222 were regrouped into indices using diagnostic pigments ($\text{DP} = \text{alloxanthin (Allo)} + 19'$ -
223 hexanoyloxyfucoxanthin (Hex) + $19'$ -butanoyloxyfucoxanthin (But) + fucoxanthin
224 (Fuco) + zeaxanthin (Zea) + chlorophyll b (Chlb) + peridinin (Peri)). They were used to follow the
225 temporal evolution of the pico- ($\text{PPF} = (\text{Zea} + \text{Chlb}) / \text{DP}$), nano- ($\text{NPF} = (\text{Hex} + \text{But} + \text{Allo}) / \text{DP}$),
226 and microphytoplankton ($\text{MPF} = (\text{Fuco} + \text{Peri}) / \text{DP}$) proportion factors (Hooker et al., 2005;
227 Vidussi et al., 2001). PPF and NPF compared well with pico- ($R^2 = 0.97$, $n = 9$) and
228 nanophytoplankton ($R^2 = 0.84$, $n = 9$) cell abundances measured by flow cytometry, respectively.

229 **2.3.3. Photochemical efficiency**

230 The maximum quantum yield of photosystem II (F_v/F_m) was measured on a Fast Repetition
231 Rate fluorometer (Chelsea Technologies Group Fast Ocean Sensor). Triplicate samples (20
232 mL) were taken from each incubation bottle and dark-adapted for 30 min. F_v/F_m (where $F_v =$
233 $F_m - F_0$) was estimated from F_0 and F_m , which refer to the minimum and maximum
234 fluorescence in the dark-acclimated state, respectively.

235 **2.3.4. Secondary production**

236 Bacterial production (BP) was estimated by the ^3H -Leucine incorporation method (Kirchman
237 et al., 1985) adapted by Smith and Azam (1992) for measuring bacterial production directly in
238 microcentrifuge tubes. Briefly, 1.5 mL samples were incubated in the dark at in situ
239 temperature for 2–3 h with a mixture of radioactive (L-[3,4,5- ^3H (N)] PerkinElmer, specific
240 activity $123.8 \text{ mCi}\cdot\text{mol}^{-1}$) and nonradioactive leucine (20 nM final concentration). Incubations
241 were started within 10 min of collection and maintained at in situ surface temperature (13.5°C).
242 Samples were run with two replicates and one trichloroacetic acid (TCA; Sigma)-killed control
243 (5% [vol/vol] final concentration). At the end of the incubation time, 200 μL of 50% TCA is
244 added to all but the control tubes to terminate leucine incorporation. Samples were centrifuged

245 at 16,000g for 10 min, the supernatant discarded, and the resultant precipitated cells were
246 washed by the addition of 1.5 ml of 5% TCA and vortex mixing. Samples were centrifuged
247 again (16,000g for 10 min) and the supernatant was removed. Subsequently, 1.5 mL of
248 UltimaGold™ uLLt (PerkinElmer) was added to each tubes, mixed, and allowed to sit for
249 >24 h before the radioactivity was counted onboard in Hidex 300SL Liquid Scintillation
250 Counter. The linearity of leucine incorporation was tested in parallel. Details for the calculation
251 can be found in a companion paper (Fourquez et al., 2020).

252 **2.3 Chemical analysis**

253 Dissolved inorganic nutrients were analysed on board with a segmented flow analyser (AIII
254 HR Seal Analytical) according to Rees et al. (2019). Detection limits were 0.02 μM for P, 0.02
255 μM for N, and 0.2 μM for Si. DFe was analyzed by flow injection with online preconcentration
256 and chemiluminescence detection (adapted from Obata et al., 1993). The detection limit was
257 40 pM and the accuracy of the method was controlled by analyzing the SAFe S (0.11 ± 0.04
258 nmol kg^{-1} ($n = 3$); consensus value $0.093 \pm 0.008 \text{ nmol kg}^{-1}$), and SAFe D1 ($0.66 \pm 0.06 \text{ nmol}$
259 kg^{-1} ($n = 4$); consensus value $0.67 \pm 0.04 \text{ nmol kg}^{-1}$) standards. Iron organic speciation was
260 measured by Competitive Ligand Exchange-Adsorptive Cathodic Stripping Voltammetry as
261 per Abualhaija & van den Berg (2014).

262 **3 Results and discussion**

263 Eddie's can develop as a closed structure with no other possible inputs of DFe to the upper
264 ocean than of new (from deep waters) or regenerated DFe (from remineralization). The
265 contribution of new Fe to total Fe supply — the f_e ratio (new Fe/(new + regenerated Fe)) —
266 thus can range between 6% and 50% from low- to high-DFe waters (Tagliabue et al., 2014 and
267 refs herein). In this context, our study aimed to provide a mechanistic understanding of the
268 biological response to ML deepening when cells are adapted to strong Fe limitation and
269 hypothetical low f_e ratio. To define the biological context of our experiments and to determine
270 whether biological parameters in our experiments were similar to those sampled in the field,
271 we start by discussing the initial conditions of our study.

272 **3.1 Initial conditions**

273 **3.1.1 Surface**

274 In-eddy, surface DFe levels were exceedingly low (<50 pM), and Chl *a* and primary
275 productivity were about 1.5 and 3 times lower, respectively than surrounding Subantarctic
276 waters (Ellwood et al., 2020; Moreau et al., 2017). We sampled the microbial community at
277 the center of the eddy, and the photosynthetic competence of the cells was relatively high at
278 the initial time of sampling ($F_v/F_m = 0.47 \pm 0.07$; Fig. 1b). It is a surprising result when
279 considering that under DFe limitation and replenished macronutrients (Suppl. Table 1), the
280 F_v/F_m ratio decreases proportionally with the degree of Fe stress (Falkowski & Kolber, 1995;
281 Greene et al., 1994). Nevertheless, relatively high F_v/F_m does not necessarily reflect Fe-replete
282 conditions for cells as it can also be indicative of a ‘signature’ for taxonomic composition of
283 the phytoplankton community (Suggett et al., 2009). Within the eddy, small photosynthetic
284 cells (< 2 μ m) – including cyanobacteria – dominated Fe uptake in the total community (Suppl.
285 Table 2, Ellwood et al. 2020). But for cyanobacteria F_0 does not arise from photosystem II
286 alone, and the baseline fluorescence from phycobilisomes and photosystem I can significantly
287 contribute to the F_0 signal (Campbell et al., 1998; Murphy et al., 2017; Simis et al., 2012).
288 Therefore, in this context the values of fluorescence-based parameters that use F_0 in their
289 calculation, such as F_v/F_m ratio, must be interpreted with knowledge of the composition and
290 evolution of the community.

291 In-eddy, cumulative Fe uptake of phytoplankton cells was approximately four orders of
292 magnitude higher than the diffusion supply rate of new Fe across the euphotic zone (Ellwood
293 et al., 2020), thus cells were probably highly reliant upon recycled Fe by different members of
294 the microbial community. In the Southern Ocean, the pool of biogenic Fe in surface waters can
295 be recycled by the action of grazers (Strzepek et al., 2005; Sarthou et al., 2008), viruses
296 (Bonnain et al., 2016; Poorvin et al., 2011) and bacteria (Fourquez et al., 2020; Strzepek et al.,
297 2005). A closer look at the distribution of these classes of organisms is therefore relevant for
298 this study. Within the mixed layer (0-100m) zooplankton abundance and biomass were
299 substantially higher within the eddy relative to the edge (Suppl. Fig. 3). For bacteria, cell
300 abundance was on average (0-300m) 3 times higher at the edge ($1.32 \pm 0.26 \times 10^6$ cells mL⁻¹,
301 $n=7$) than at the center of the eddy ($0.43 \pm 0.22 \times 10^6$ cells mL⁻¹, $n=5$); and in relative to the total
302 assemblage, the number of HNA bacteria were also found to be higher at the edge ($56 \pm 11\%$
303 HNA) while LNA bacteria were more prominent in the center of the Eddy ($95 \pm 2\%$ LNA).
304 Surprisingly, BP was the highest at the center of the eddy (Suppl. Fig 4), and even more than
305 5 times greater than rates measured at the edge when normalized by cell abundance (Suppl.
306 Figure 4b). This result was unexpected as it goes against the widespread theory of LNA being

307 inactive cells, whereas HNA are usually regarded as the active part of the bacterial group
308 (Lebaron et al., 2001). However, high growth-specific rates for LNA in nutrient-limited waters
309 contradict this view in the past (Zubkov et al., 2001). This marked discrepancy between the
310 proportion of HNA and BP rates in our study demonstrate that LNA bacteria are an active part
311 of microbial communities. One possible explanation is the profound impact of grazing on the
312 abundance of HNA in favour of LNA (Hu et al., 2020). Importantly, these results bear the
313 stamp of intense bacterial and grazing activities, which may have led to the recycling of Fe
314 (and the concurrent release of Fe-binding ligands) in the upper layer.

315 **3.1.2 Subsurface**

316 In this study, we used freshly regenerated DFe from subsurface particles to mimic resupply via
317 diapycnal diffusion (Fe-REG treatment, see Suppl. Fig. 1). Using particulate Fe (PFe)
318 concentration at 150m depth (0.025nM, data not shown) in conjunction with the particle
319 concentration factor, we estimated that 16% of the PFe was transferred to the dissolved phase
320 after 6 days. In the natural environment, the partitioning between particulate and dissolved Fe
321 phases can result from biotic recycling and abiotic dissolution processes. Here, there are several
322 lines of evidence to suggest that biotic actions were at play. An increase in bacterial production
323 (BP) for particle attached-bacteria confirms that they were metabolically active (Suppl. Fig. 5).
324 The increase in ammonium concentration (Suppl. Fig. 5), the most commonly regenerated
325 product (Bronk et al., 2007), further confirms that remineralization took place rapidly after the
326 resuspension of the particles. There was also indirect evidence of relatively rapid bacterial
327 consumption of Fe, but the quasi-linear temporal trend in DFe concentration suggests a
328 constant release rate (Suppl. Fig 5f).

329 Microbial remineralization of organic matter also supplies ligands, which can form complexes
330 with newly regenerated DFe, keeping it in solution (Boyd & Ellwood, 2010; Bressac et al.,
331 2019). There are previous reports of the concurrent release of weak Fe-binding ligands during
332 particle remineralization experiments (Bundy et al., 2016; Velasquez et al., 2016; Whitby et
333 al., 2020). In these studies, grazers may have played an important role in releasing both
334 intracellular Fe and ligands, as well as modifying their composition thereby affecting Fe
335 chemistry and bioavailability (Boyd et al., 2005, 2012). The release of predation during the
336 preparation of regenerated DFe source (section 2.2.2) would have altered the grazer-mediated
337 regeneration of Fe, likely dominant within the eddy - based on microzooplankton biomass
338 (Supp. Fig. 2) - and more broadly in the Subantarctic (Bowie et al., 2001; Boyd et al., 2005,

339 2010; Evans & Brussaard, 2012; Sarthou et al., 2008). Thus, we cannot rule out that the amount
340 of DFe regenerated may have been less, relative to that *in situ*, during the incubation of particles
341 with no grazers. However, we can reasonably assume that viral abundance was not affected by
342 the resuspension of particles in viral-replete (i.e., <0.2 μm filtered) seawater (e.g., Cram et al.,
343 2016). Therefore, we consider the 16% regeneration rate derived as a lower estimate, especially
344 because a significant amount of the Fe released during the experiment (Suppl. Fig. 5-h) was
345 observed to be rapidly assimilated by the prokaryotes present.

346 **3.2 Biological responses**

347 The (subsaturating) addition of DFe and nutrients with realistic stoichiometries (Table 1 and
348 Supp. Table 1), along with the relief in grazing pressure following dilution (Landry & Hassett,
349 1982), reproduced well the perturbations experienced by natural communities over vast areas
350 during ML deepening. Biological responses are driven by a range of mechanisms, which can
351 be broadly split between phototrophic (influenced by Fe) and heterotrophic (influenced by both
352 Fe and C) responses.

353 **3.2.1 Phototrophic responses to Fe sources**

354 After 2 days, there was the first evidence of acclimation of phytoplankton with an increase in
355 Chl *a* concentration in all three treatments (Fig. 1a), and by the end of the incubation time a
356 3.5 (Fe-NO, Fe-NEW) to 5-fold (Fe-REG) increase in Chl *a* was observed (Fig. 1a). The Fe-
357 REG treatment showed the highest increase in Chl *a*, which was significantly different
358 (Student's test, $p < 0.01$) as compared to the two other treatments. No differences in Chl *a* were
359 found between Fe-NO and Fe-NEW over the time of the experiment (Fig. 1 a). Although the
360 initial phytoplankton community was dominated by nanophytoplankton (i.e., <20 μm , $64 \pm 1\%$),
361 the increase in Chl *a* by day 6 (Fig. 1a) may be attributed to an increase in the abundance of
362 picoplankton (mainly cyanobacteria, Fig. 2c) and microplankton (i.e., >20 μm). For Fe-NO and
363 Fe-NEW, the increase in diatoms biomass was clearly apparent from elevated fucoxanthin
364 pigment concentrations compared to initial conditions (Fig. 2 f). In Fe-REG treatment, the
365 response of diatoms was less pronounced (Fig. 2 f) and haptophytes were overall the major
366 components of the phytoplankton community in this treatment ($57 \pm 5\%$ by day 6). Interestingly,
367 macronutrients concentration (Suppl. Fig. 7) showed similar trends for the three treatments.
368 The initial conditions for the experiment had relatively elevated macronutrient concentrations
369 (Suppl. Table 1). Thus, the phytoplankton community was likely not macronutrient limited.
370 There was only little nitrate consumption over time, but there was significant ammonium

371 drawdown observed by day 2 of the experiment in all the treatments (Suppl. Fig. 7). We further
372 note that the drawdown in ammonium was accompanied by a significant increase in HNA cells
373 in all the incubations (Fig. 2). Among all incubation bottles and time points, the minimal value
374 in Si concentration was 2.4 μM (Suppl. Fig. 7d) which is well above limiting levels of $<1 \mu\text{M}$
375 reached in mid-summer in the Subantarctic (Bowie et al., 2009; Eriksen et al., 2018). In
376 contrast, final DFe concentrations systematically reached limiting levels of $\sim 0.1 \text{ nM}$ (Table 1)
377 which is consistent with the persistent decline in Fv/Fm (Fig. 1b).

378

379 While the algal responses to each treatment seem comparable considering differences in DFe
380 concentration at T0 (Table 1), a 10-fold range of the $\Delta\text{DFe}/\Delta\text{Chl}a$ ratio (i.e., the drawdown in
381 DFe over the increase in Chl *a*: 0.03, 0.2 and 0.3 for Fe-NO, Fe-NEW and Fe-REG,
382 respectively) points to very different trends. Those deviations in $\Delta\text{DFe}/\Delta\text{Chl}a$ could reflect the
383 capacity for luxury Fe uptake by cells (i.e. acquire Fe in excess of that required to maintain
384 maximum growth). In-eddy, phytoplankton Fe-to-carbon uptake ratios were unusually high
385 (Ellwood et al. 2020), indicating that cells upregulated their Fe acquisition machinery relative
386 to carbon (Suppl. Table 2). Therefore, phytoplankton could have consumed DFe at higher rates
387 than required when DFe level was sufficiently high without any change in biomass. Accounting
388 for the role of the different DFe inputs (source and amounts, see Table 1) in phytoplankton
389 growth requires the parallel consideration of DFe recycled during the 6 days of the experiment.

390 The relative contribution of new versus regenerated Fe to biological Fe uptake is described by
391 the *fe* ratio (Boyd et al., 2005). Based on similar considerations, we can explore the relative
392 contribution of DFe recycled (within the incubation bottle over the duration of the experiment)
393 to that of the DFe pool at time zero. This information, termed here as the “apparent *fe* ratio”,
394 is also the starting point of the discussion to explain that similar DFe concentrations were
395 measured for the three treatments by day 6 (Table 1). Since the uptake of Fe was not directly
396 measured in our experiment, our apparent *fe* ratio is computed by comparing *in situ* Fe uptake
397 rates measured on the natural communities during the same study in a companion paper
398 (Ellwood et al., 2020) versus estimates of Fe recycling rates. The apparent *fe* ratio is calculated
399 by assuming steady-state conditions and with a constant Fe uptake rate over the experiment.
400 The total amount of Fe taken up by phytoplankton was assessed by combining the *in situ* size-
401 fractionated Fe uptake rates (Supp. Table 2, Ellwood et al., 2020) with the development of the
402 pico-, nano- and micro- phytoplankton biomass obtained from a diagnostic pigment criterion
403 (section 2.3, Figure 3). The difference between the final (measured) and theoretical (estimated)

404 concentration of DFe in incubation bottles represents the amount of Fe recycled. Since the DFe
 405 concentration was measured at the start and end of the incubation, here we define the “net Fe
 406 uptake” as the difference between the two values:

$$407 \quad \text{Net DFe uptake} = \text{DFe initial} - \text{DFe final}$$

408 Where DFe initial and DFe final are the concentration of DFe measured at the start and the end of the
 409 experiment in the incubation bottle, respectively.

410 The “Net DFe uptake” can also be formulated as a combination of two other terms :

$$411 \quad \text{Net DFe uptake} = (\text{Total DFe uptake} \times t) + \text{DFe recycled}$$

412 Where Total DFe uptake is the amount of DFe consumed by all size-fractions (Suppl. Table 2) during
 413 the incubation time (t), and

$$414 \quad \text{DFe recycled} = \text{DFe final} - \text{DFe estimated}$$

415 and

$$416 \quad \text{DFe estimated} = \text{DFe initial} - (\text{Total DFe uptake} \times t)$$

417

418 Because experiments were conducted in a ‘batch system’ with no replenishment, the calculated
 419 DFe recycled also corresponds to the uptake of DFe by phytoplankton including DFe released
 420 by the recycling process that occurs in the bottles. Then, the apparent *fe* ratio is calculated
 421 according to the formula:

$$422 \quad \text{apparent } fe \text{ ratio} = \text{Recycled DFe uptake} / \text{Net DFe uptake}$$

423

424 Although variations in Fe uptake rates or the use of intracellular stored Fe might have impacted
 425 the accumulation or release of DFe (e.g., Twining et al., 2004; Wilhelm et al., 2013), this
 426 exercise highlights a wide-ranging apparent *fe* ratio: 0.3 (Fe-REG), 0.5 (Fe-NO) and 0.7 (Fe-
 427 NEW). An apparent *fe* ratio of 0.5 indicates that an equal amount of recycled DFe will be
 428 biologically consumed relative to the initial DFe concentration. In the Fe-NO treatment, equal
 429 values in DFe concentration between the initial and final time-points also underlines a perfect
 430 balance between Fe uptake and Fe recycling rates, demonstrating that the rapid *in situ* turnover
 431 time of the biotic Fe pool (<1 day; Ellwood et al., 2020) was not (or only temporally) affected
 432 by dilution, and pointing to the high resilience of the ferrous wheel.

433

434 **3.2.2 Heterotrophic responses to Fe sources**

435 Bacteria showed pronounced increases in abundance in all three treatments (Fig. 2a and b). An
436 increase of HNA abundance (Fig. 2b) and a constant number of bacteria with low nucleic acid
437 content (LNA) were noted during the first 4 days of incubation. The persistent increase in the
438 relative proportion of bacteria with high nucleic acid content (HNA, section 3.4), Chl *a*, and
439 cell abundance may indicate that the grazer population did not recover completely from
440 dilution after 6 days of incubation (Fig. 1a and 2). The relative proportion of HNA cells
441 increased from 2-4% at the initial time to 11% (Fe-NO) and 43-36% (Fe-NEW and Fe-REG,
442 respectively) at day 2 and went on increasing up to about 60% by day 4 in all treatments (Fig
443 2b). Overall, stimulation in bacterial production rates, potentially driven by metabolically more
444 active HNA bacteria, may have led to the recycling of Fe (and the concurrent release of Fe-
445 binding ligands) similarly to what was observed during the preparation of Fe regenerated
446 source from subsurface particles. Finally, we observed a decreasing trend starting on day 4 and
447 the percentage of HNA cells accounted for less than 10% of the cells in all treatments by the
448 end of the experiment.

449 Knowledge of the environmental controls on bacteria is needed to interpret these results from
450 the three treatments. In high nutrients low chlorophyll (HNLC) regions, both Fe and C may be
451 present at limiting concentrations for heterotrophic bacteria (Church et al., 2000; Fourquez et
452 al., 2020; Obernosterer et al., 2015), leading to interactions among different bacterial groups
453 to access Fe (Fourquez et al., 2012, 2016). The primary dependence of bacterial growth by one
454 or the other element also directly influences interactions between primary producers and
455 bacteria (Fourquez et al., 2015, 2020). In our study, an increase in BP rates were observed in
456 the dark treatments (NO-dark, REG-dark, NO-dark +C), and the absence of stimulation after
457 the addition of Fe (NO-dark +Fe) indicate that bacteria were primarily C-limited (Fig. 1d). The
458 highest BP rates were observed when both C and Fe were added (NO-dark +Fe+C; Fig. 1d),
459 supporting previous observations of increasing bacterial Fe demand when C limitation is
460 relieved (Fourquez et al., 2014). A tight coupling between phytoplankton and bacteria biomass
461 also confirms that bacterial growth was mainly driven by the release of phytoplankton-derived
462 dissolved organic C (DOC) in the incubation bottles (Fig. 4). Assuming that the release of
463 phytoplankton-derived DOC followed a trend similar to the initial DFe concentrations, the
464 expected enhancement bacterial Fe uptake that would result in the Fe-NEW and Fe-REG
465 treatments could explain the wide range in $\Delta\text{DFe}/\Delta\text{Chla}$ ratio (section 3.3.1). However,
466 replenished organic C-conditions for bacteria also exacerbate competition for Fe with pico-
467 nanophytoplankton cells (Fourquez et al., 2020), and fast-growing heterotrophic bacteria (i.e.

468 HNA) may quickly shift to Fe limitation. If this scenario occurs, the remineralisation process
469 would be compromised which ultimately reduce the amount of Fe recycled from bacterial
470 activities (Fourquez et al., 2020).

471 **3.2.3 Is biogenic Fe recycled available to all biota?**

472 The preferential response of the phytoplankton biomass relative to bacteria in the Fe-REG
473 treatment (Fig. 4) suggests that autotrophic cells, likely haptophytes (as revealed by algal
474 pigment data), consumed most of the added DFe. Within the eddy, the increased importance of
475 Fe recycling favours smaller phytoplankton cells, which is reflected in terms of cell
476 abundances, size-fractionated Fe uptake and the Fe:C uptake ratio datasets (Suppl. Table 2).
477 Picophytoplankton cells were about 20% more abundant in Fe-REG than in the other two
478 treatments by the end of the experiment (day 6, Fig. 2d), and this difference was significant
479 (Student's test, $p < 0.01$). Similar observations can be made for nanophytoplankton as we
480 measured higher cell abundances in Fe-REG treatment starting from day 2 (Fig. 2e). In
481 contrast, a relatively modest increase in the contribution of diatoms to Chl *a* biomass was
482 observed, starting from ~15% and reaching <30% 6 days later (Fig. 2f). Interestingly, this
483 increase was the lowest in the Fe-REG treatment, where the initial DFe concentration exceeded
484 the putative DFe threshold of 0.2 nM required for diatoms to alleviate Fe stress (Boyd et al.,
485 2012). This departure from theory may reflect the inability of diatoms to outcompete pico- and
486 nanophytoplankton for regenerated DFe. Thus, despite diatoms requiring little Fe to bloom
487 (Boyd et al., 2012; Strzepek et al., 2011, 2019) they could not access enough regenerated Fe to
488 exploit the available macronutrients in the Fe-REG treatment (i.e. $6.07 \pm 0.07 \mu\text{M SiOH}_4$,
489 Suppl. Table 1). The inability of diatoms to utilize this source of Fe, or at least at a lower rate
490 than non-diatoms cells (i.e. smaller cells) may be attributed to their physico-chemical
491 disadvantages (e.g. lower surface area: ratio and diffusion rates), but it may also be due to the
492 bioavailability of DFe following ligand complexation in the Fe-REG treatment.

493 At the start of the experiment, we measured the highest concentration in ligands for the Fe-
494 REG treatment (Table 1). These ligands were present in a large excess of total DFe in the Fe-
495 REG treatment (0.26 nM of DFe and 2.04 nM ligands) and were defined as predominantly
496 weak ligands ($\log K_{\text{Fe}^{\text{L}}} < 12$, Table 1). It should be noted that, contrary to weak ligands, strong
497 ligands ($\log K_{\text{Fe}^{\text{L}}} > 12$) decrease Fe bioavailability and are typically used to define the lower
498 limit of Fe bioavailability in phytoplankton-based uptake assay (Lis et al., 2015). The release
499 of both strong and weak Fe-binding ligands by the heterotrophic community were measured

500 during previous subsurface ocean remineralization experiments (Bundy et al., 2016; Velasquez
501 et al., 2016). In our study, there was no detection of type L1 strong ligands by electrochemical
502 analysis. The same analytical technique was employed in Velasquez et al. (2016) but the
503 authors showed that it failed to detect L1 from their samples, although siderophores (which
504 have conditional stability constants comparable to greater than L1 ligands [Vraspir & Butler,
505 2009]) were detected by mass spectrometry. The ligands associated with particle breakdown
506 also tend to have lower conditional stability constants ($\log K_{Fe'L}$ 10–12, or < 10 , Boyd et al.,
507 2010; Hassler et al., 2017). It is probable that particle-associated siderophores were present at
508 very low concentrations in the Fe-REG treatment. Their contribution to the ligands pool may
509 be too small compared to other weaker organic ligands to be detected by the method. Given
510 that it is not clear what properties of ligands dictate the bioavailability of Fe, it is difficult to
511 draw conclusions here. However, it is well admitted that a loosely defined fraction of DFe, the
512 inorganic Fe (Fe'), can effectively be taken up by all microorganisms to support their
513 metabolism and growth (C. S. Hassler et al., 2012; Morel et al., 2008). We calculated Fe' in all
514 three treatments (Table 1), and although Fe' concentration represented systematically less than
515 1% of total DFe and was not enough to satisfy the biological demand, we still note that at initial
516 times there was respectively 1.7 and 3 times more Fe' in Fe-REG than in Fe-NEW and Fe-NO
517 treatments.

518 **3.2.4 How well do bacteria to sustain phytoplankton with remineralization?**

519 Towards the end of summer, when f_e ratio is supposedly low, steady-state conditions are
520 maintained by intense recycling of Fe. The short residence time of less than one day calculated
521 in Ellwood et al. (2020) argues that Fe is being heavily trafficked within the euphotic zone.
522 When scaled to the in-eddy inventory, such a high resilience in the ferrous wheel and the wide-
523 ranging efficiency of Fe recycling highlights the role of bacteria. In this study we indirectly
524 evaluate their efficiency at recycling Fe in incubations experiment. An alternative approach to
525 exploring Fe recycling through bacterial activities is using the carbon budget. Estimates of
526 organic C remineralization rates ($C\text{-remin} = BCD/PP*100$) are deduced from BP rates,
527 bacterial carbon demand (BCD) and net primary production (NPP) rates integrated over the
528 euphotic zone (100m). BCD was estimated assuming a bacterial growth efficiency (BGE) of
529 0.10 that was measured during the same study (Fourquez et al. 2020). For full details
530 concerning the assessment of BP and BCD we refer to Fourquez et al. (2020). Here we calculate
531 that 11% of the NPP were remineralized by heterotrophic bacteria. Assuming that the fraction

532 of Fe remineralized is the same as that of C (Bowie et al., 2015; Sarthou et al., 2008), we can
533 conclude that similar fractions of NPP and Fe-demand are remineralized, and thus using the %
534 of NPP that is remineralized and results from Fe-uptake experiments, we can obtain an estimate
535 of Fe regeneration rate. Hence, this Fe regenerated rate was $0.94 \text{ pmol L}^{-1} \text{ d}^{-1}$ which represents
536 about 7% of the total Fe uptake integrated over the euphotic layer ($12.8 \text{ pmol L}^{-1} \text{ d}^{-1}$, Ellwood
537 et al. 2020), meaning that our estimate of DFe supply from remineralization cannot meet the
538 entire Fe demand. Nevertheless, it could either meet 40% or 43% of the Fe demand by small
539 phytoplankton cells ($2\text{-}20\mu\text{m} - 2.35 \text{ pmol L}^{-1} \text{ d}^{-1}$) or large phytoplankton cells ($>20\mu\text{m} - 2.18$
540 $\text{pmol L}^{-1} \text{ d}^{-1}$), respectively. The timescale of Fe recycling is inextricably linked to the turnover
541 times of the members of the microbial community, explained by growth and mortality rates.
542 The role of grazers is partially precluded by our experimental approach but those of viruses
543 need to be considered. Although not measured in this study, viruses, unaffected by the dilution,
544 can contribute as much as grazers to Fe recycling in HNLC regions (Poorvin et al., 2004;
545 Strzepek et al., 2005, Boyd and Ellwood, 2010; Boyd et al., 2012). Viral lysis may rapidly lead
546 to the remobilization of their intracellular Fe within the ferrous wheel, in agreement with the
547 rapid turnover time of the biogenic Fe pool.

548 **4 CONCLUSIONS**

549 In the Southern Ocean, decades of studies have demonstrated that in addition to physical DFe
550 supply, Fe bioavailability for cells is under tight control by chemistry. To date, describing the
551 bioavailability of Fe in these waters relies on the accuracy of the chemical methods used to
552 measure DFe (as referred to as bioavailable) at vanishing low concentrations. But the concept
553 of “bioavailability” is bound to be nebulous because light, Fe speciation and kinetics,
554 temperature, microbial interactions and adaptations are all, and more elements, intertwined into
555 the definition. However, it is possible to indirectly constrain Fe bioavailability by tracking the
556 biological responses to the supply of different forms of DFe and ligands. Here, we demonstrate
557 that DFe regenerated from particles and new DFe was not beneficial to the same phytoplankton
558 taxon. We also show that resident cells, with low f_e ratios at the end of the summer, can rapidly
559 shift from surface recycling to regenerated DFe or new Fe over the timescale of day. This shift
560 in the mode of Fe recycling is partly induced by the competitive advantage of small cells
561 (prokaryotes and picophytoplankton) to access DFe. These interspecific interactions,
562 exacerbated by the partial relief in grazing pressure driven by the dilution from ML deepening,
563 prevent diatoms growing and favors the rapid remobilization of intracellular Fe within the

564 ferrous wheel. In addition, the plasticity of the autotrophic metabolic machinery and the
565 potential role played by bacteria, as a major component of the biotic Fe pool, can further limit
566 the effect of vertical Fe supply. Together, these mechanisms buffer the response of
567 phytoplankton biomass to vertical Fe supply despite extremely low ambient DFe levels in areas
568 where control by grazing is prominent such as the Subantarctic.

569 **Acknowledgements** – This study is part of the EDDY project supported under Australian
570 Research Council’s Special Research Initiative for Antarctic Gateway Partnership (Project ID
571 SR140300001). M.F. was funded from the European Union’s Horizon 2020 research and
572 innovation programme under the Marie Skłodowska-Curie grant agreement N° 894264
573 (BULLE-project). This project was also funded by a Marie Skłodowska-Curie Postdoctoral
574 European Fellowship awarded to M.B. (European Union Seventh Framework Programme -
575 FP7/2007-2013) under grant agreement no. PIOF-GA-2012-626734. The authors wish to thank
576 the CSIRO Marine National Facility (MNF) for its support in the form of sea time on RV
577 *Investigator*, support personnel, scientific equipment and data management. We particularly
578 thank Cassie Schwanger for nutrient analyses onboard. All data and samples acquired on the
579 voyage are made publicly available in accordance with MNF policy. The authors also wish to
580 thank the CSIRO Hydrochemistry team, A. Davidson, and S. Moreau for their help in
581 sample/data analyses and Ingrid Obernosterer for her valuable comments on the manuscript.

582 **5 References**

- 583 Abualhaija, M. M., & van den Berg, C. M. G. (2014). Chemical speciation of iron in seawater
 584 using catalytic cathodic stripping voltammetry with ligand competition against
 585 salicylaldoxime. *Marine Chemistry*, *164*, 60–74.
 586 <https://doi.org/10.1016/J.MARCHEM.2014.06.005>
- 587 Arteaga, L. A., Boss, E., Behrenfeld, M. J., Westberry, T. K., & Sarmiento, J. L. (2020).
 588 Seasonal modulation of phytoplankton biomass in the Southern Ocean. *Nature*
 589 *Communications*, *11*(1). <https://doi.org/10.1038/s41467-020-19157-2>
- 590 Behrenfeld, M. J. (2010). Abandoning Sverdrup's Critical Depth Hypothesis on phytoplankton
 591 blooms. *Ecology*, *91*(4), 977–989. <https://doi.org/10.1890/09-1207.1>
- 592 Blain, S., & Tagliabue, A. (2016). *Iron Cycle in Oceans*. John Wiley & Sons, Incorporated.
 593 <https://doi.org/10.1002/9781119136859>
- 594 Bonnain, C., Breitbart, M., & Buck, K. N. (2016). The Ferrojan horse hypothesis: Iron-virus
 595 interactions in the ocean. *Frontiers in Marine Science*, *3*(JUN), 1–11.
 596 <https://doi.org/10.3389/fmars.2016.00082>
- 597 Bowie, A. R., Maldonado, M. T., Frew, R. D., Croot, P. L., Achterberg, E. P., Mantoura, R. F.
 598 C., et al. (2001). The fate of added iron during a mesoscale fertilisation experiment in the
 599 Southern Ocean. *Deep Sea Research Part II: Topical Studies in Oceanography*, *48*(11–
 600 12), 2703–2743. [https://doi.org/10.1016/S0967-0645\(01\)00015-7](https://doi.org/10.1016/S0967-0645(01)00015-7)
- 601 Bowie, A. R., Van Der Merwe, P., Qu  rou  , F., Trull, T., Fourquez, M., Planchon, F., et al.
 602 (2015). Iron budgets for three distinct biogeochemical sites around the Kerguelen
 603 archipelago (Southern Ocean) during the natural fertilisation experiment KEOPS-2.
 604 *Biogeosciences*, *12*(12), 4421–4445. <https://doi.org/10.5194/bg-12-4421-2015>
- 605 Boyd, P. W. (2002). Environmental factors controlling phytoplankton processes in the
 606 Southern Ocean. *Journal of Phycology*, *86*(1), 844–861.
- 607 Boyd, P. W., & Abraham, E. R. (2001). Iron-mediated changes in phytoplankton
 608 photosynthetic competence during SOIREE. *Deep Sea Research Part II*, *48*, 2529–2550.
- 609 Boyd, P. W., & Ellwood, M. J. (2010). The biogeochemical cycle of iron in the ocean. *Nature*
 610 *Geoscience*, *3*(10), 675–682. <https://doi.org/10.1038/ngeo964>
- 611 Boyd, P. W., Law, C. S., Hutchins, D. A., Abraham, E. R., Croot, P. L., Ellwood, M., et al.
 612 (2005). FeCycle: Attempting an iron biogeochemical budget from a mesoscale SF 6 tracer
 613 experiment in unperturbed low iron waters. *Global Biogeochemical Cycles*, *19*(4), 1–13.
 614 <https://doi.org/10.1029/2005GB002494>

- 615 Boyd, P. W., Ibsanmi, E., Sander, S. G., Hunter, K. A., & Jackson, G. A. (2010).
616 Remineralization of upper ocean particles: Implications for iron biogeochemistry.
617 *Limnology and Oceanography*, 55(3), 1271–1288. Retrieved from
618 http://www.aslo.org/lo/toc/vol_55/issue_3/1271.html
- 619 Boyd, P. W., Arrigo, K. R., Strzepek, R., & Van Dijken, G. L. (2012). Mapping phytoplankton
620 iron utilization: Insights into Southern Ocean supply mechanisms. *Journal of Geophysical*
621 *Research: Oceans*, 117(C6), n/a-n/a. <https://doi.org/10.1029/2011JC007726>
- 622 Boyd, P. W., Ellwood, M. J., Tagliabue, A., & Twining, B. S. (2017). Biotic and abiotic
623 retention, recycling and remineralization of metals in the ocean. *Nature Geoscience*,
624 10(3), 167–173. <https://doi.org/10.1038/ngeo2876>
- 625 Bressac, M., Guieu, C., Ellwood, M. J., Tagliabue, A., Wagener, T., Laurenceau-Cornec, E.
626 C., et al. (2019). Resupply of mesopelagic dissolved iron controlled by particulate iron
627 composition. *Nature Geoscience* 2019 12:12, 12(12), 995–1000.
628 <https://doi.org/10.1038/s41561-019-0476-6>
- 629 Bronk, D. A., See, J. H., Bradley, P., & Killberg, L. (2007). DON as a source of bioavailable
630 nitrogen for phytoplankton. *Biogeosciences*, 4(3), 283–296. [https://doi.org/10.5194/BG-](https://doi.org/10.5194/BG-4-283-2007)
631 [4-283-2007](https://doi.org/10.5194/BG-4-283-2007)
- 632 Bundy, R. M., Jiang, M., Carter, M., & Barbeau, K. A. (2016). Iron-binding ligands in the
633 Southern California current system: Mechanistic studies. *Frontiers in Marine Science*,
634 3(MAR), 1–17. <https://doi.org/10.3389/fmars.2016.00027>
- 635 Campbell, D., Hurry, V., Clarke, A. K., Gustafsson, P., & Öquist, G. (1998). Chlorophyll
636 fluorescence analysis of cyanobacterial photosynthesis and acclimation. *Microbiology*
637 *and Molecular Biology Reviews: MMBR*, 62(3), 667–683.
638 <https://doi.org/10.1128/MMBR.62.3.667-683.1998>
- 639 Church, M. J., Hutchins, D. A., & Ducklow, H. W. (2000). Limitation of bacterial growth by
640 dissolved organic matter and iron in the Southern Ocean. *Applied and Environmental*
641 *Microbiology*, 66(2), 455–466. <https://doi.org/10.1128/AEM.66.2.455-466.2000>
- 642 Cram, J. A., Parada, A. E., & Fuhrman, J. A. (2016). Dilution reveals how viral lysis and
643 grazing shape microbial communities. *Limnology and Oceanography*, 61(3), 889–905.
644 <https://doi.org/10.1002/LNO.10259>
- 645 Cutter, G., Sciences, A., Dominion, O., Casciotti, K., Croot, P., Sciences, O., et al. (2017).
646 Sampling and Sample-handling Protocols for GEOTRACES Cruises, (August).
- 647 Ellwood, M. J., Strzepek, R. F., Strutton, P. G., Trull, T. W., Fourquez, M., & Boyd, P. W.
648 (2020). Distinct iron cycling in a Southern Ocean eddy. *Nature Communications*, 11(1).

- 649 <https://doi.org/10.1038/s41467-020-14464-0>
- 650 Evans, C., & Brussaard, C. P. D. (2012). Viral lysis and microzooplankton grazing of
651 phytoplankton throughout the Southern Ocean. *Limnology and Oceanography*, 57(6),
652 1826–1837. <https://doi.org/10.4319/LO.2012.57.6.1826>
- 653 Falkowski, P. G., & Kolber, Z. (1995). Variations in Chlorophyll Fluorescence Yields in
654 Phytoplankton in the World Oceans. *Functional Plant Biology*, 22(2), 341–355.
655 <https://doi.org/10.1071/PP9950341>
- 656 Fauchereau, N., Tagliabue, A., Bopp, L., Monteiro, P., & S Monteiro, P. M. (2011). The
657 response of phytoplankton biomass to transient mixing events in the Southern Ocean The
658 response of phyto-plankton biomass to transient mixing events in the The response of
659 phytoplankton biomass to transient mixing events in the Southern Ocean. *Geophysical*
660 *Research Letters*, 38(17). <https://doi.org/10.1029/2011GL048498>
- 661 Fourquez, M., Obernosterer, I., & Blain, S. (2012). A method for the use of the radiotracer
662 ⁵⁵Fe for microautoradiography and CARD-FISH of natural bacterial communities. *FEMS*
663 *Microbiology Letters*, 337(2), 132–139. <https://doi.org/10.1111/1574-6968.12022>
- 664 Fourquez, M., Schaumann, A., Gueneugues, A., Jouenne, T., & Obernosterer, I. (2014). Effects
665 of iron limitation on growth and carbon metabolism in oceanic and coastal heterotrophic
666 bacteria. *Limnology and Oceanography*, 59(1), 1–14.
667 <https://doi.org/10.4319/lo.2014.59.1.0000>
- 668 Fourquez, M., Obernosterer, I., Davies, D. M., Trull, T. W., & Blain, S. (2015). Microbial iron
669 uptake in the naturally fertilized waters in the vicinity of the Kerguelen Islands:
670 phytoplankton–bacteria interactions. *Biogeosciences*. [https://doi.org/10.5194/bg-12-](https://doi.org/10.5194/bg-12-1893-2015)
671 1893-2015
- 672 Fourquez, M., Beier, S., Jongmans, E., Hunter, R., & Obernosterer, I. (2016). Uptake of
673 Leucine, Chitin, and Iron by Prokaryotic Groups during Spring Phytoplankton Blooms
674 Induced by Natural Iron Fertilization off Kerguelen Island (Southern Ocean). *Frontiers in*
675 *Marine Science*, 3, 256. <https://doi.org/10.3389/fmars.2016.00256>
- 676 Fourquez, M., Bressac, M., Deppeler, S. L., Ellwood, M., Obernosterer, I., Trull, T. W., et al.
677 (2020). Microbial Competition in the Subpolar Southern Ocean : An Fe – C Co-limitation
678 Experiment. *Frontiers in Marine Science*, 6(January), 776.
679 <https://doi.org/10.3389/fmars.2019.00776>
- 680 Frenger, I., Münnich, M., Gruber, N., & Knutti, R. (2015). Southern Ocean eddy
681 phenomenology. *Journal of Geophysical Research: Oceans*, 120(11), 7413–7449.
682 <https://doi.org/10.1002/2015JC011047>

- 683 Greene, R. M., Kolber, Z. S., Swift, D. G., Tindale, N. W., & Falkowski, P. G. (1994).
 684 Physiological limitation of phytoplankton photosynthesis in the eastern equatorial Pacific
 685 determined from variability in the quantum yield of fluorescence. *Limnology and*
 686 *Oceanography*, 39(5), 1061–1074. <https://doi.org/10.4319/LO.1994.39.5.1061>
- 687 Hassler, C. S., Schoemann, V., Boye, M., Tagliabue, A., Rozmarynowycz, M., & McKay, R.
 688 M. L. (2012). Iron bioavailability in the southern ocean. *Oceanography and Marine*
 689 *Biology: An Annual Review*, 50, 1–64. [https://doi.org/10.1201/B12157-3/IRON-](https://doi.org/10.1201/B12157-3/IRON-BIOAVAILABILITY-SOUTHERN-OCEAN-HASSLER-SCHOEMANN-BOYE-TAGLIABUE-ROZMARYNOWYCZ-MCKAY)
 690 [BIOAVAILABILITY-SOUTHERN-OCEAN-HASSLER-SCHOEMANN-BOYE-](https://doi.org/10.1201/B12157-3/IRON-BIOAVAILABILITY-SOUTHERN-OCEAN-HASSLER-SCHOEMANN-BOYE-TAGLIABUE-ROZMARYNOWYCZ-MCKAY)
 691 [TAGLIABUE-ROZMARYNOWYCZ-MCKAY](https://doi.org/10.1201/B12157-3/IRON-BIOAVAILABILITY-SOUTHERN-OCEAN-HASSLER-SCHOEMANN-BOYE-TAGLIABUE-ROZMARYNOWYCZ-MCKAY)
- 692 Hassler, Christel S., van den Berg, C. M. G., & Boyd, P. W. (2017). Toward a regional
 693 classification to provide a more inclusive examination of the ocean biogeochemistry of
 694 iron-binding ligands. *Frontiers in Marine Science*, 4(FEB).
 695 <https://doi.org/10.3389/fmars.2017.00019>
- 696 Hooker, S. B., Van Heukelem, L., Thomas, C. S., Claustre, H., Ras, J., Barlow, R., et al. (2005).
 697 The Second SeaWiFS HPLC Analysis Round-Robin Experiment (SeaHARRE-2).
 698 *National Aeronautics and Space Administration, Goddard Space Flight Center.*, 212785,
 699 112. Retrieved from <http://www.sti.nasa.gov/STI-homepage.html>
- 700 Hu, C., Chen, X., Yu, L., Xu, D., & Jiao, N. (2020). Elevated Contribution of Low Nucleic
 701 Acid Prokaryotes and Viral Lysis to the Prokaryotic Community Along the Nutrient
 702 Gradient From an Estuary to Open Ocean Transect. *Frontiers in Microbiology*,
 703 11(December), 1–14. <https://doi.org/10.3389/fmicb.2020.612053>
- 704 Hudson, R. J. M., & Morel, F. M. M. (1990). Iron transport in marine phytoplankton: Kinetics
 705 of cellular and medium coordination reactions. *Limnology and Oceanography*, 35(5),
 706 1002–1020.
- 707 Hunter, K. A., & Boyd, P. W. (2007). Iron-binding ligands and their role in the ocean
 708 biogeochemistry of iron. *Environmental Chemistry*, 4(4), 221.
 709 <https://doi.org/10.1071/EN07012>
- 710 Kirchman, D. L. (1996). Microbial ferrous wheel. *Nature*, 383, 303–304.
- 711 Kirchman, D. L., K'nees, E., & Hodson, R. (1985). Leucine incorporation and its potential as
 712 a measure of protein synthesis by bacteria in natural aquatic systems. *Applied and*
 713 *Environmental Microbiology*, 49(3), 599–607. Retrieved from
 714 [http://www.pubmedcentral.nih.gov/articlerender.fcgi?artid=373556&tool=pmcentrez&r-](http://www.pubmedcentral.nih.gov/articlerender.fcgi?artid=373556&tool=pmcentrez&rendertype=abstract)
 715 [endertype=abstract](http://www.pubmedcentral.nih.gov/articlerender.fcgi?artid=373556&tool=pmcentrez&rendertype=abstract)
- 716 Landry, M. R., & Hassett, R. P. (1982). Estimating the grazing impact of marine micro-

- 717 zooplankton. *Marine Biology* 1982 67:3, 67(3), 283–288.
718 <https://doi.org/10.1007/BF00397668>
- 719 Lebaron, P., Servais, P., Agogu e, H., Courties, C., & Joux, F. (2001). Does the high nucleic
720 acid content of individual bacterial cells allow us to discriminate between active cells and
721 inactive cells in aquatic systems? *Applied and Environmental Microbiology*, 67(4), 1775–
722 1782. <https://doi.org/10.1128/AEM.67.4.1775-1782.2001>
- 723 Lis, H., Shaked, Y., Kranzler, C., Keren, N., & Morel, F. M. M. (2015). Iron bioavailability to
724 phytoplankton: an empirical approach. *ISME Journal*, 9(4), 1003–1013.
725 <https://doi.org/10.1038/ismej.2014.199>
- 726 Moore, J., Doney, S., Glover, D., & Fung, I. (2001). Iron cycling and nutrient-limitation
727 patterns in surface waters of the World Ocean. *Deep Sea Research Part II*, 49(1–3), 463–
728 507. Retrieved from <http://linkinghub.elsevier.com/retrieve/pii/S0967064501001096>
- 729 Moreau, S., Penna, A. Della, Llort, J., Patel, R., Langlais, C., Boyd, P. W., et al. (2017). Eddy-
730 induced carbon transport across the Antarctic Circumpolar Current. *Global*
731 *Biogeochemical Cycles*, 31(9), 1368–1386. <https://doi.org/10.1002/2017GB005669>
- 732 Morel, F. M. M., Kustka, A. B., & Shaked, Y. (2008). The role of unchelated Fe in the iron
733 nutrition of phytoplankton. *Limnology and Oceanography*, 53(1), 400–404.
- 734 Mtshali, T. N., van Horsten, N. R., Thomalla, S. J., Ryan-Keogh, T. J., Nicholson, S. A.,
735 Roychoudhury, A. N., et al. (2019). Seasonal Depletion of the Dissolved Iron Reservoirs
736 in the Sub-Antarctic Zone of the Southern Atlantic Ocean. *Geophysical Research Letters*,
737 46(8), 4386–4395. <https://doi.org/10.1029/2018GL081355>
- 738 Murphy, C. D., Ni, G., Li, G., Barnett, A., Xu, K., Grant-Burt, J., et al. (2017). Quantitating
739 active photosystem II reaction center content from fluorescence induction transients.
740 *Limnology and Oceanography: Methods*, 15(1), 54–69.
741 <https://doi.org/10.1002/LOM3.10142>
- 742 Nicholson, S. A., L evy, M., Jouanno, J., Capet, X., Swart, S., & Monteiro, P. M. S. (2019).
743 Iron Supply Pathways Between the Surface and Subsurface Waters of the Southern Ocean:
744 From Winter Entrainment to Summer Storms. *Geophysical Research Letters*, 46(24),
745 14567–14575. <https://doi.org/10.1029/2019GL084657>
- 746 Nunn, B. L., Faux, J. F., Hippmann, A. a., Maldonado, M. T., Harvey, H. R., Goodlett, D. R.,
747 et al. (2013). Diatom Proteomics Reveals Unique Acclimation Strategies to Mitigate Fe
748 Limitation. *PLoS ONE*, 8(10), e75653. <https://doi.org/10.1371/journal.pone.0075653>
- 749 Obernosterer, I., Fourquez, M., & Blain, S. (2015). Fe and C co-limitation of heterotrophic
750 bacteria in the naturally fertilized region off the Kerguelen Islands. *Biogeosciences*,

- 751 12(11), 1983–1992. <https://doi.org/10.5194/bg-12-1983-2015>
- 752 Patel, R. S., Phillips, H. E., Strutton, P. G., Lenton, A., & Llorc, J. (2019). Meridional Heat and
753 Salt Transport Across the Subantarctic Front by Cold-Core Eddies. *Journal of*
754 *Geophysical Research: Oceans*, 124(2), 981–1004.
755 <https://doi.org/10.1029/2018JC014655>
- 756 Poorvin, L., Rinta-Kanto, J. M., Hutchins, D. A., & Wilhelm, S. W. (2004). Viral release of
757 iron and its bioavailability to marine plankton. *Limnology and Oceanography*, 49(5),
758 1734–1741. <https://doi.org/10.4319/lo.2004.49.5.1734>
- 759 Poorvin, L., Sander, S. G., Velasquez, I., Ibisanni, E., LeClerc, G. R., & Wilhelm, S. W. (2011).
760 A comparison of Fe bioavailability and binding of a catecholate siderophore with virus-
761 mediated lysates from the marine bacterium *Vibrio alginolyticus* PWH3a. *Journal of*
762 *Experimental Marine Biology and Ecology*, 399(1), 43–47.
763 <https://doi.org/10.1016/J.JEMBE.2011.01.016>
- 764 Rembauville, M., Briggs, N., Ardyna, M., Uitz, J., Catala, P., Penkerch, C., et al. (2017).
765 Plankton Assemblage Estimated with BGC-Argo Floats in the Southern Ocean:
766 Implications for Seasonal Successions and Particle Export. *Journal of Geophysical*
767 *Research: Oceans*, 122(10), 8278–8292. <https://doi.org/10.1002/2017JC013067>
- 768 Ryan-Keogh, T. J., Thomalla, S. J., Little, H., & Melanson, J. R. (2018). Seasonal regulation
769 of the coupling between photosynthetic electron transport and carbon fixation in the
770 Southern Ocean. *Limnology and Oceanography*, 63(5), 1856–1876.
771 <https://doi.org/10.1002/lno.10812>
- 772 Saito, M. A., Bertrand, E. M., Dutkiewicz, S., Bulygin, V. V., Moran, D. M., Monteiro, F. M.,
773 et al. (2011). Iron conservation by reduction of metalloenzyme inventories in the marine
774 diazotroph *Crocospaera watsonii*. *Proceedings of the National Academy of Sciences of*
775 *the United States of America*, 108(6), 2184–2189.
776 <https://doi.org/10.1073/pnas.1006943108>
- 777 Sarthou, G., Vincent, D., Christaki, U., Obernosterer, I., Timmermans, K. R., & Brussaard, C.
778 P. D. (2008). The fate of biogenic iron during a phytoplankton bloom induced by natural
779 fertilisation: Impact of copepod grazing. *Deep Sea Research Part II*, 55(5–7), 734–751.
780 <https://doi.org/10.1016/j.dsr2.2007.12.033>
- 781 Simis, S. G. H., Huot, Y., Babin, M., Seppälä, J., & Metsamaa, L. (2012). Optimization of
782 variable fluorescence measurements of phytoplankton communities with cyanobacteria.
783 *Photosynthesis Research*, 112(1), 13–30. [https://doi.org/10.1007/S11120-012-9729-](https://doi.org/10.1007/S11120-012-9729-6)
784 [6/FIGURES/12](https://doi.org/10.1007/S11120-012-9729-6)

- 785 Smith, D. C., & Azam, F. (1992). A simple , economical method for measuring bacterial protein
786 synthesis rates in seawater using 3H-leucine. *Marine Microbial Food Webs*, 6(2), 107–
787 114.
- 788 Strzepek, R. F., & Harrison, P. J. (2004). Photosynthetic architecture differs in coastal and
789 oceanic diatoms. *Nature*, 403, 689–692. <https://doi.org/10.1038/nature02954>
- 790 Strzepek, R. F., Maldonado, M. T., Higgins, J. L., Hall, J., Safi, K., Wilhelm, S. W., & Boyd,
791 P. W. (2005). Spinning the “Ferrous Wheel”: The importance of the microbial community
792 in an iron budget during the FeCycle experiment. *Global Biogeochemical Cycles*, 19(4),
793 1–14. <https://doi.org/10.1029/2005GB002490>
- 794 Strzepek, R. F., Maldonado, M. T., Hunter, K. A., Frew, R. D., & Boyd, P. W. (2011). Adaptive
795 strategies by Southern Ocean phytoplankton to lessen iron limitation: Uptake of
796 organically complexed iron and reduced cellular iron requirements. *Limnology and*
797 *Oceanography*, 56(6), 1983–2002. <https://doi.org/10.4319/lo.2011.56.6.1983>
- 798 Strzepek, R. F., Boyd, P. W., & Sunda, W. G. (2019). Photosynthetic adaptation to low iron,
799 light, and temperature in Southern Ocean phytoplankton. *Proceedings of the National*
800 *Academy of Sciences of the United States of America*, 116(10), 4388–4393.
801 <https://doi.org/10.1073/pnas.1810886116>
- 802 Suggett, D. J., Moore, C. M., Hickman, A. E., & Geider, R. J. (2009). Interpretation of fast
803 repetition rate (FRR) fluorescence: Signatures of phytoplankton community structure
804 versus physiological state. *Marine Ecology Progress Series*, 376(May 2014), 1–19.
805 <https://doi.org/10.3354/meps07830>
- 806 Tagliabue, A., Sallée, J. B., Bowie, A. R., Lévy, M., Swart, S., & Boyd, P. W. (2014). Surface-
807 water iron supplies in the Southern Ocean sustained by deep winter mixing. *Nature*
808 *Geoscience*, 7(4), 314–320. <https://doi.org/10.1038/ngeo2101>
- 809 Thomalla, S. J., Fauchereau, N., Swart, S., & Monteiro, P. M. S. (2011). Regional scale
810 characteristics of the seasonal cycle of chlorophyll in the Southern Ocean.
811 *Biogeosciences*, 8(10), 2849–2866. <https://doi.org/10.5194/BG-8-2849-2011>
- 812 Toulza, E., Tagliabue, A., Blain, S., & Piganeau, G. (2012). Analysis of the global ocean
813 sampling (GOS) project for trends in iron uptake by surface ocean microbes. *PloS One*,
814 7(2), e30931. <https://doi.org/10.1371/journal.pone.0030931>
- 815 Twining, B. S., & Baines, S. B. (2013). The trace metal composition of marine phytoplankton.
816 *Annual Review of Marine Science*, 5, 191–215. <https://doi.org/10.1146/annurev-marine-121211-172322>
- 817
818 Velasquez, I. B., Ibsanmi, E., Maas, E. W., Boyd, P. W., Nodder, S., & Sander, S. G. (2016).

- 819 Ferrioxamine siderophores detected amongst iron binding ligands produced during the
820 remineralization of marine particles. *Frontiers in Marine Science*, 3(SEP), 1–14.
821 <https://doi.org/10.3389/fmars.2016.00172>
- 822 Vidussi, F., Claustre, H., Manca, B. B., Luchetta, A., & Marty, J. C. (2001). Phytoplankton
823 pigment distribution in relation to upper thermocline circulation in the eastern
824 Mediterranean Sea during winter. *Journal of Geophysical Research: Oceans*, 106(C9),
825 19939–19956. <https://doi.org/10.1029/1999JC000308>
- 826 Vraspir, J. M., & Butler, A. (2009). Chemistry of Marine Ligands and Siderophores. *Annual*
827 *Review of Marine Science*, 1(1), 43–63. Retrieved from
828 <http://www.annualreviews.org/doi/abs/10.1146/annurev.marine.010908.163712>
- 829 Whitby, H., Bressac, M., Sarthou, G., Ellwood, M. J., Guieu, C., & Boyd, P. W. (2020).
830 Contribution of Electroactive Humic Substances to the Iron-Binding Ligands Released
831 During Microbial Remineralization of Sinking Particles. *Geophysical Research Letters*,
832 47(7). <https://doi.org/10.1029/2019GL086685>
- 833 Wright, S. W., van den Enden, R. L., Pearce, I., Davidson, A. T., Scott, F. J., & Westwood, K.
834 J. (2010). Phytoplankton community structure and stocks in the Southern Ocean (30–
835 80°E) determined by CHEMTAX analysis of HPLC pigment signatures. *Deep Sea*
836 *Research Part II: Topical Studies in Oceanography*, 57(9–10), 758–778.
837 <https://doi.org/10.1016/J.DSR2.2009.06.015>
- 838 Zubkov, M. V., Fuchs, B. M., Burkill, P. H., & Amann, R. (2001). Comparison of Cellular and
839 Biomass Specific Activities of Dominant Bacterioplankton Groups in Stratified Waters of
840 the Celtic Sea. *Applied and Environmental Microbiology*, 67(3–12), 5210–5218.
841 <https://doi.org/10.1128/AEM.67.11.5210-5218.2001>
842

Table 1. Initial and final concentrations in dissolved iron (DFe), inorganic Fe (Fe'), total iron-binding ligand (LT), and conditional stability constants ($\log K'_{\text{Fe}'\text{L}}$). Values within parentheses correspond to the standard deviation of the mean of three measurements. ND denotes no data.

Treatment	DFe (nM)		LT (nM)		Log $K'_{\text{Fe}'\text{L}}$		Fe' (pM)	
	Initial	Final	Initial	Final	Initial	Final	Initial	Final
Fe-NO	0.11 (0.01)	0.11 (0.01)	1.36 (0.13)	ND	11.0 (0.3)	ND	0.80 (0.1)	ND
Fe-NEW	0.16 (0.04)	0.09 (0.01)	1.69 (0.21)	ND	10.8 (0.3)	ND	1.49 (0.4)	ND
Fe-REG	0.26 (0.02)	0.10 (0.01)	2.04 (0.11)	ND	10.7 (0.2)	ND	2.52 (0.1)	ND

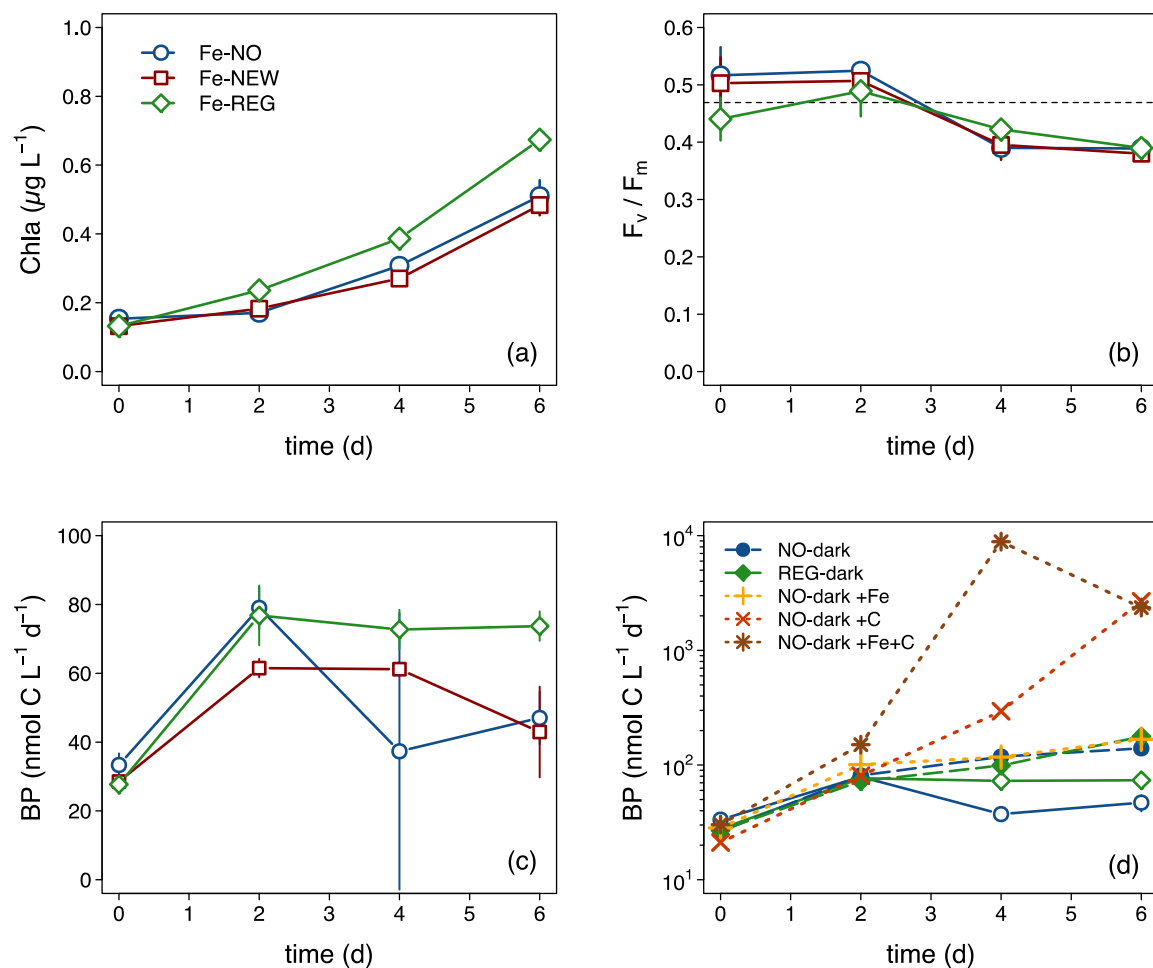


Figure 1. Time evolution of (a) Chla concentration, (b) F_v/F_m ratio, and (c) bacterial production (BP) for the three treatments. The horizontal dotted line in (b) corresponds to the *in situ* F_v/F_m ratio. (d) Time evolution of BP for Fe-NO and Fe-REG incubated under light and dark (NO-dark, REG-dark) conditions, and for amended (+Fe, +C, +Fe+C) NO-dark treatments. Note the logarithmic scale for the y-axis in (d). Error bars represent the standard deviation of three incubation bottle replicates.

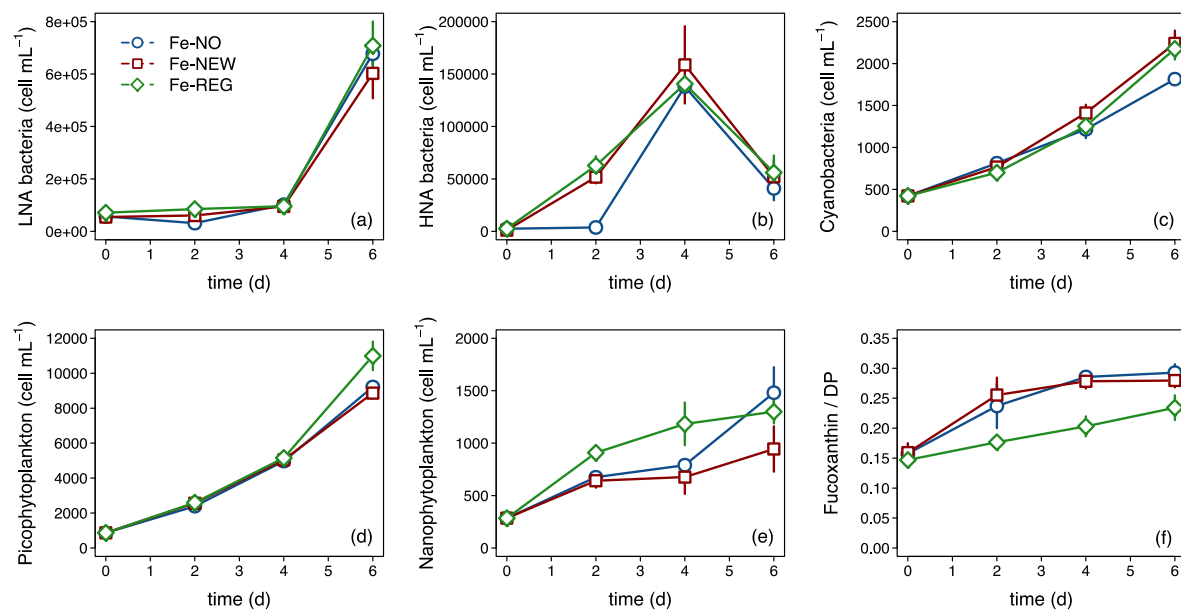


Figure 2. Time evolution of the abundance of (a) LNA bacteria, (b) HNA bacteria, (c) cyanobacteria, (d) picophytoplankton, and (e) nanophytoplankton measured by flow cytometry. (f) Time evolution of the Fucoxanthin/DP ratio, a proxy of the relative proportion of diatoms to total algal biomass derived from pigment analysis (section 2.2). Error bars represent the standard deviation of three incubation bottle replicates.

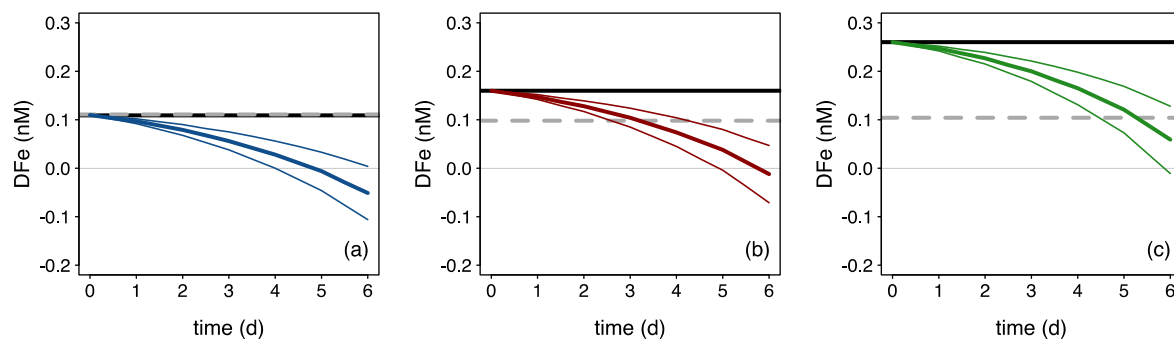


Figure 3. Theoretical evolution of DFe driven by phytoplankton uptake (colored curves) for the (a) Fe-NO, (b) Fe-NEW, and (c) Fe-REG treatments. Theoretical evolutions of DFe are represented in color lines: blue, red and green for the Fe-NO, Fe-NEW and Fe-REG treatments, respectively and were obtained by combining the *in situ* size-fractionated Fe uptakes rates (Supp. Table 2) with the evolution of the pico-, nano- and microphytoplankton biomass obtained from a diagnostic pigment criteria (section 2.2). The black and grey-dotted lines represent the measured initial and final DFe concentrations, respectively.

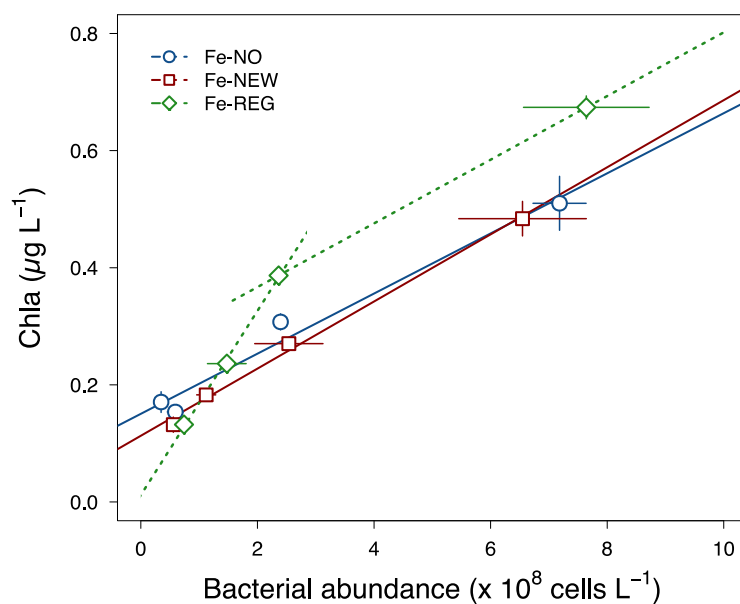


Figure 4. Relationship between Chla concentration and bacterial abundance (HNA+LNA) for the three treatments. The best-fit lines of the linear models are plotted (Fe-NO: slope = $5.1 \pm 0.6 \times 10^{-10}$, $R^2 = 0.98$, $p = 0.01$; Fe-NEW: slope = $5.7 \pm 0.3 \times 10^{-10}$, $R^2 = 0.99$, $p = 0.002$; Fe-REG day 0-4: slope = $15.7 \pm 0.8 \times 10^{-10}$, $R^2 = 0.99$, $p = 0.3$; Fe-REG day 4-6: slope = 5.4×10^{-10}). Error bars represent the standard deviation of three incubation bottle replicates.

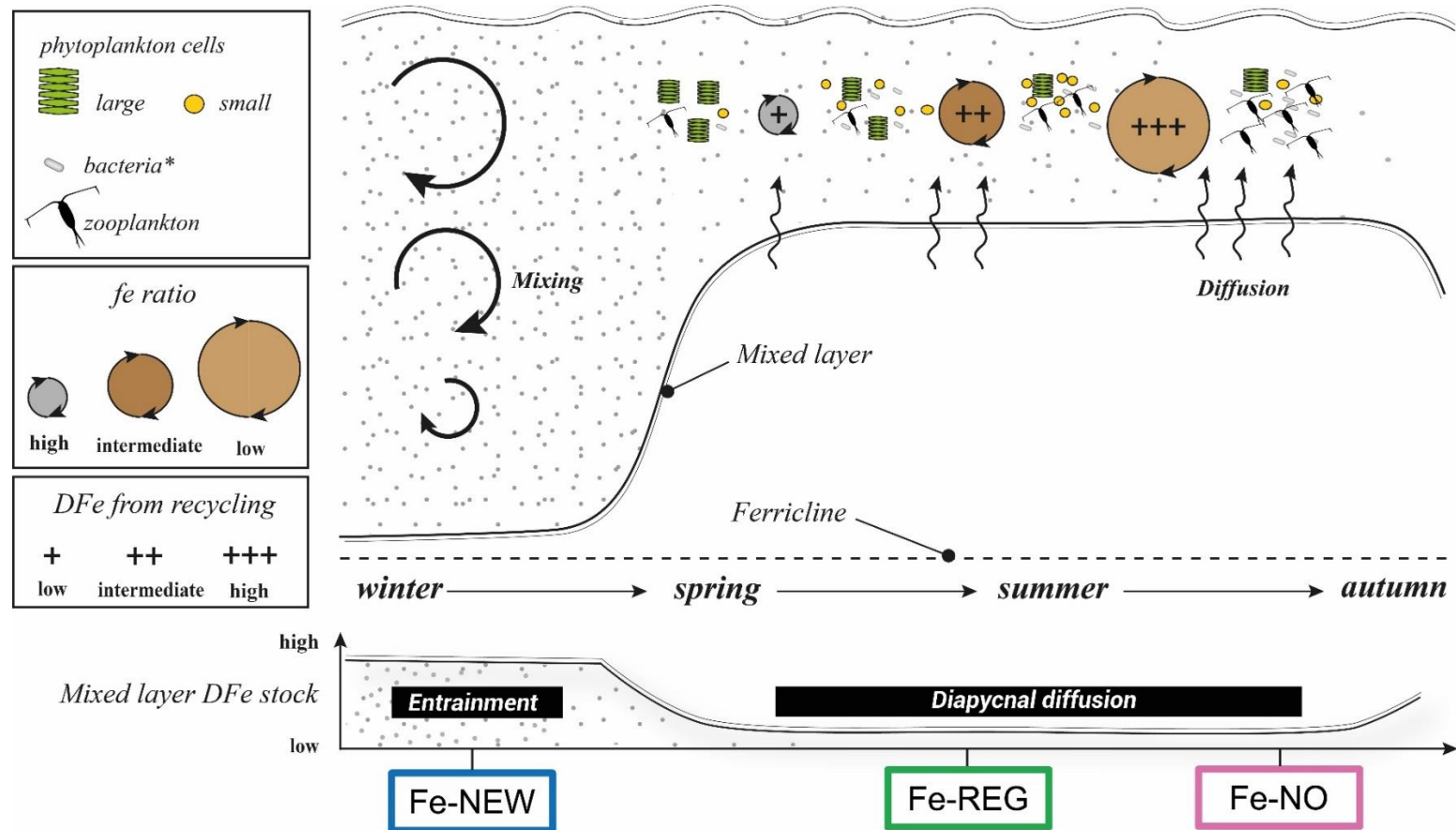
Suppl. Table 1. Initial biogeochemical conditions for the Fe-NO, Fe-NEW, and Fe-REG treatments.

	Fe-NO	Fe-NEW	Fe-REG
Ammonium (μM)	1.22 ± 0.16	0.72 ± 0.24	1.03 ± 0.34
Nitrate (μM)	22.36 ± 0.76	23.26 ± 0.17	23.20 ± 0.03
Nitrite (μM)	0.35 ± 0.07	0.44 ± 0.01	0.45 ± 0.01
Phosphate (μM)	1.62 ± 0.06	1.68 ± 0.01	1.69 ± 0.01
Silicate (μM)	3.16 ± 0.08	5.43 ± 0.01	6.07 ± 0.07
Dissolved iron (nM)	0.11 ± 0.01	0.16 ± 0.04	0.26 ± 0.02
Chlorophyll-a ($\mu\text{g L}^{-1}$)	0.154 ± 0.016	0.132 ± 0.015	0.132 ± 0.003
F_v/F_m	0.52 ± 0.05	0.50 ± 0.05	0.44 ± 0.04

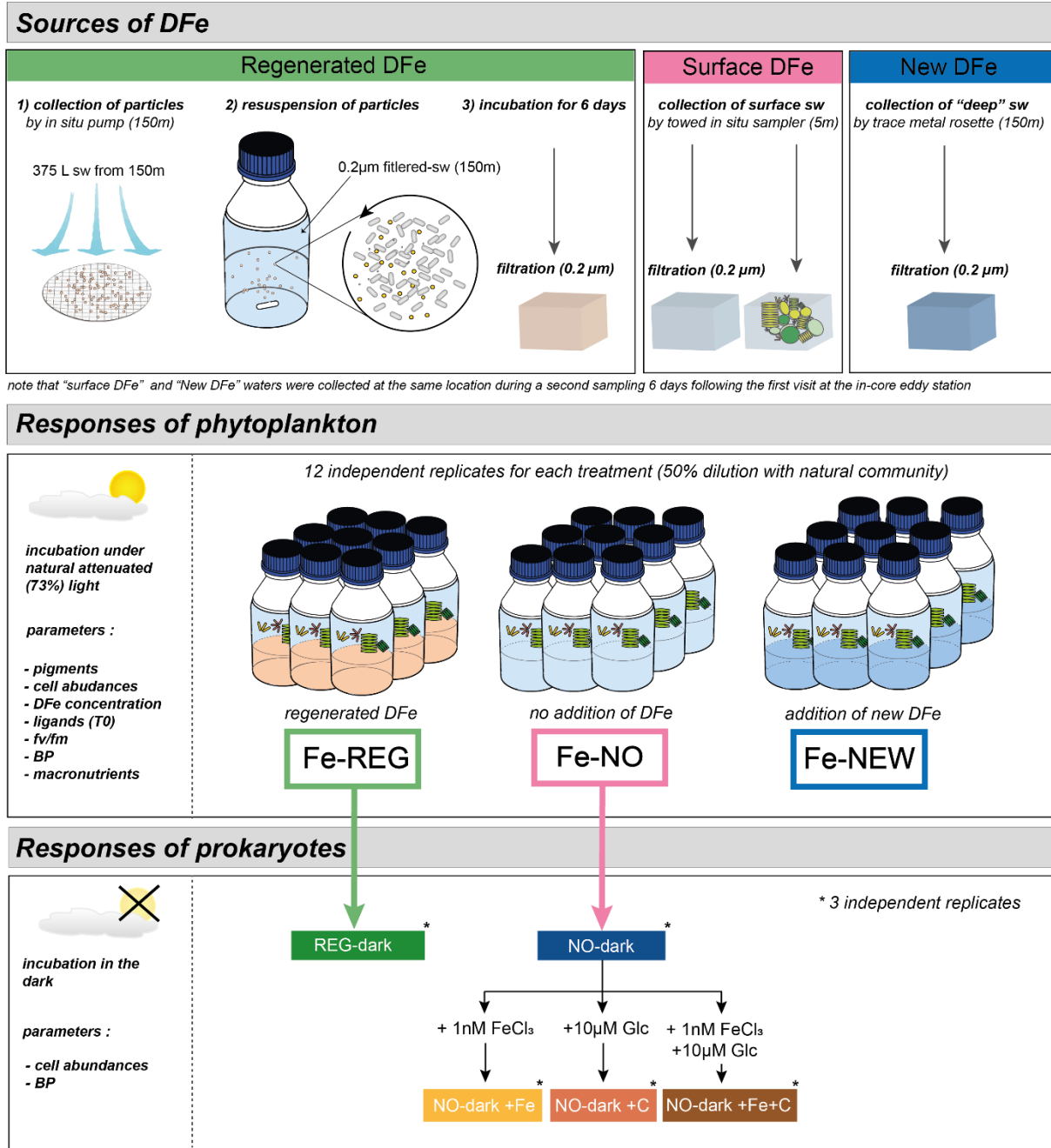
Suppl. Table 2. Iron and carbon uptake rates for the different components of the in-eddy phytoplankton community (from companion paper Ellwood et al. 2020).

	0.2-2- $\mu\text{m}^{\text{a,b}}$	2-20- $\mu\text{m}^{\text{a,b}}$	>20- $\mu\text{m}^{\text{a,b}}$
Fe uptake ($\text{pmol L}^{-1} \text{d}^{-1}$)	17.4 (5.6)	4.6 (3.0)	4.9 (1.2)
C uptake ($\mu\text{mol L}^{-1} \text{d}^{-1}$)	0.06 (0.01)	0.05 (0.03)	0.04 (0.01)
Fe:C ratio ($\mu\text{mol mol}^{-1}$)	285.4 (92.5)	99.6 (88.9)	120.6 (43.3)

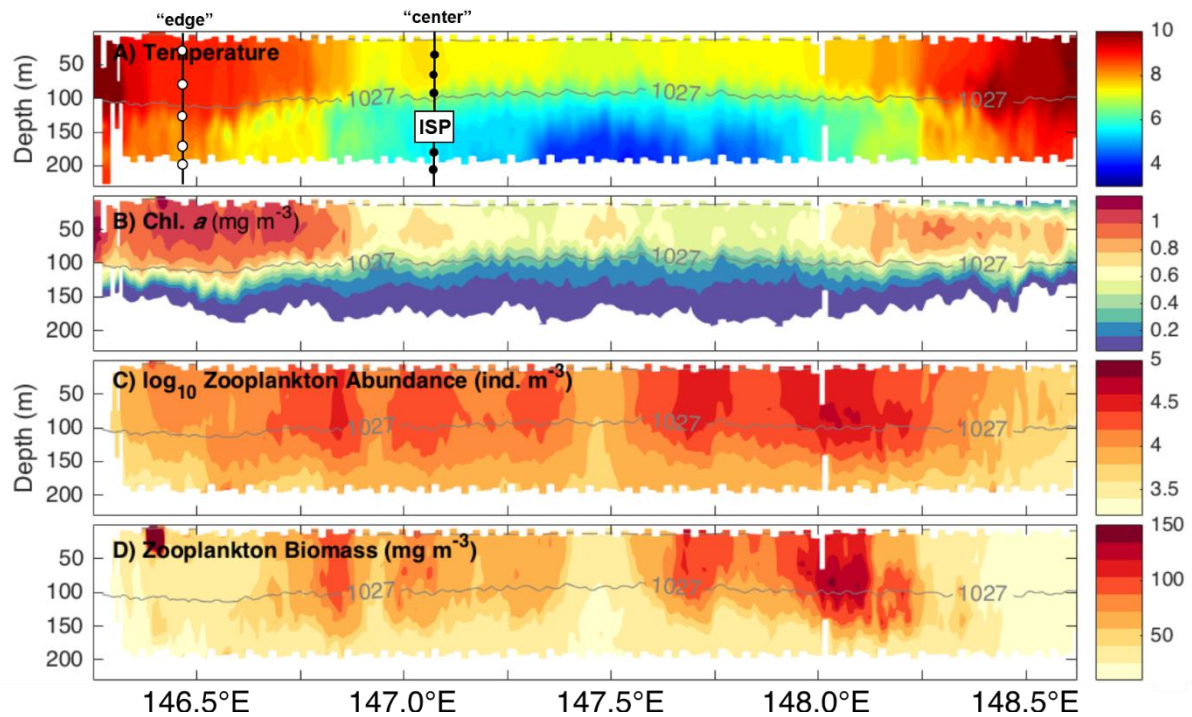
^a incubation at 80% incident irradiance; ^b extracellular Fe removed using Ti(III) EDTA-citrate



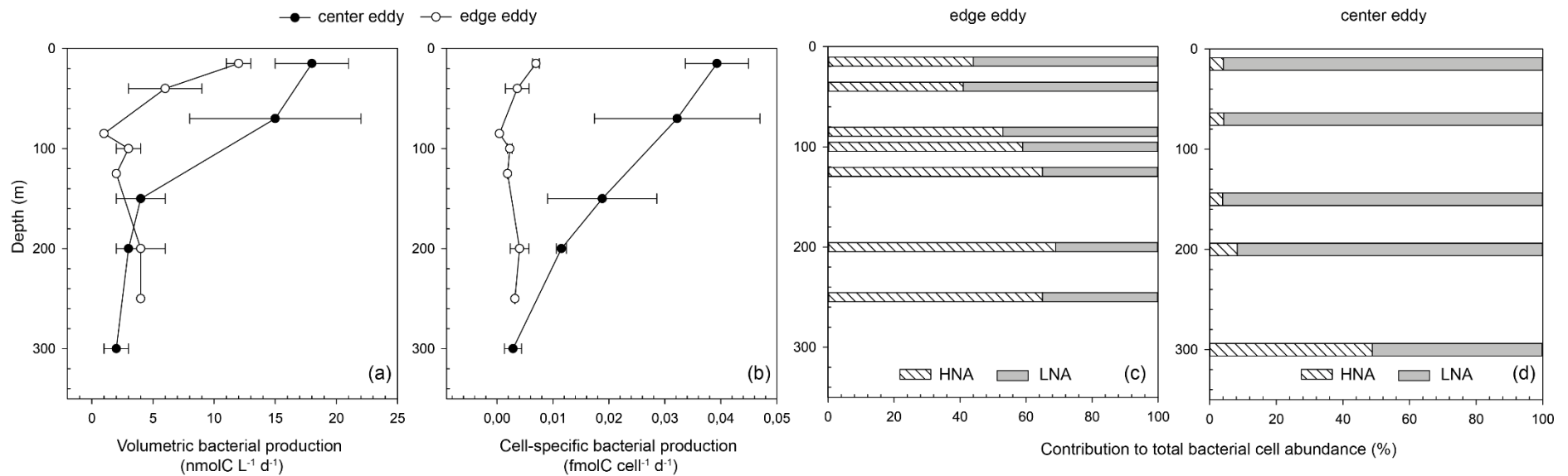
Suppl. Figure 1 A schematic representation of the seasonal variability in Southern Ocean Fe cycling adapted from Tagliabue et al. 2014. Seasonal changes in the physical supply of DFe (black arrows), mixed-layer depth and the mixed-layer DFe inventory are emphasized. The magnitude of recycling and changes in *fe* ratio are presented together (circles and cross) as well as a simplified view of the pelagic community composition. The dominant physical processes over the season is conceptualized at the bottom of the figure with the evolution of DFe inventories in the mixed layer. DFe sources (Fe-NEW, Fe-REG, and Fe-NO) used in this study aim to represent the seasonal transition of modes of DFe supply from mainly new DFe early in the season (entrainment) to regenerated DFe from recycle of sinking materials later during the summer (diapycnal diffusion) and no DFe supply.



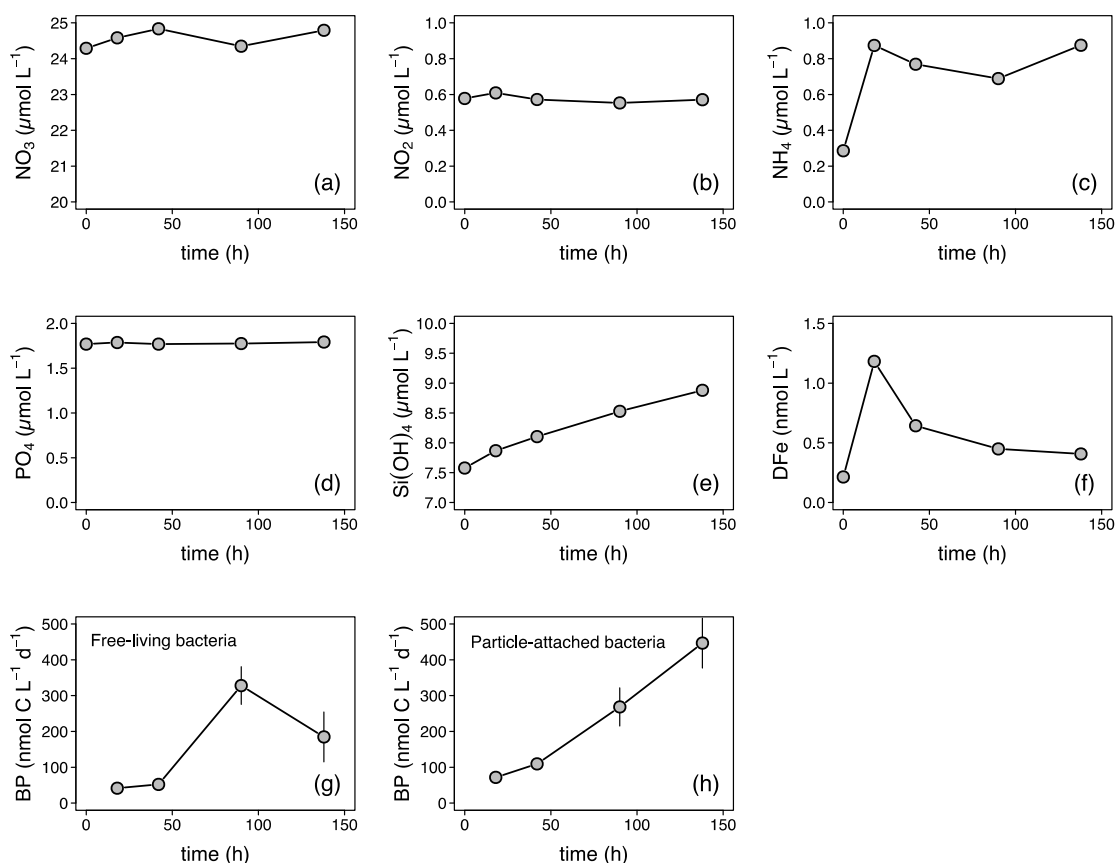
Suppl. Figure 2. A schematic representation of the experimental set-up.



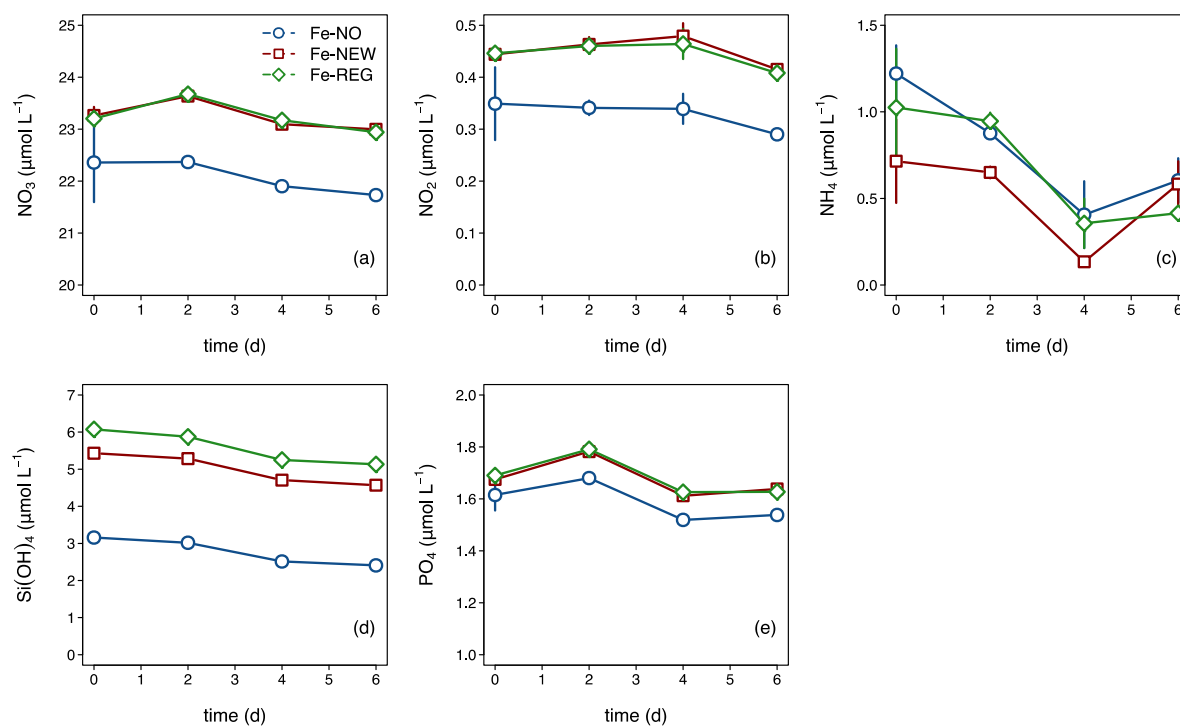
Suppl. Figure 3 (a) Temperature, (b) Chl. a concentration, and zooplankton (c) abundance and (d) biomass (obtained from a Laser Optical Plankton Recorder) within the cold-core eddy and at the eddy's periphery. Location of the sampling for bacterial production profiles at the periphery ("edge", white dots) and at the within the eddy ("center", black dots) are shown in (a) panel. Sampling for surface (5m) microbial community was done at same location within the eddy ("center") as the collection of subsurface particles by In Situ Pump (ISP) deployed at 150m depth.



Suppl. Figure 4 Depth profiles of bacterial production and abundance at the center and at the edge of the eddy. Profiles of volumetric (a) and cell-specific (relative to cell abundance) bacterial production (b) versus depth. Error bars represent 1 standard deviation for replicate measurements. Percent of relative contribution of high DNA content (HNA) and low DNA content (LNA) cells to total bacterial abundance at the edge (c) and center (d) of the eddy.



Suppl. Figure 5. Time evolution of dissolved (a) nitrate, (b) nitrite, (c) ammonium, (d) phosphate, (e) silicate, and (f) iron concentrations, and production by (g) free-living and (h) particle-attached heterotrophic bacteria during the remineralization of subsurface particles (section 2.1). Particle-attached BP was obtained by subtracting the free-living (<1- μm) from the total (unfiltered) BP.



Suppl. Figure 7. Time evolution of dissolved inorganic (a) nitrate, (b) nitrite, (c) ammonium, (d) silicate, and (e) phosphate concentrations during the incubation. Error bars represent the standard deviation of three incubation bottle replicates.